ANTIOXIDANTS & REDOX SIGNALING
Volume 24, Number 17, 2016

DOI: 10.1089/ars.2015.6505

Therapeutics

ORIGINAL RESEARCH COMMUNICATION

An Endothelial Hsp70-TLR4 Axis Limits Nox3 Expression and Protects Against Oxidant Injury in Lungs

Yi Zhang,[1] Peiying Shan,[1] Anup Srivastava,[1] Ge Jiang,[1] Xuchen Zhang,[2] and Patty J. Lee[1]

Abstract

Aims: Oxidants play a critical role in the pathogenesis of acute lung injury (ALI). Nox3 is a novel member of the NADPH oxidase (Nox) family of oxidant-generating enzymes, which our laboratory had previously identified to be induced in the lungs of *TLR4*$^{-/-}$ mice. However, the physiologic role of Nox3 induction in lungs and its precise relationship to TLR4 are unknown. Furthermore, the cell compartment involved and the signaling mechanisms of Nox3 induction are unknown. ***Results:*** We identified that Nox3 is regulated by heat shock protein 70 (Hsp70) signaling *via* a TLR4-Trif-signal transducer and activator of transcription 3 (Stat3) pathway and that Nox3 induction leads to increased oxidant injury and death in mice and lung endothelial cells. We generated *Nox3*$^{-/-}$*/TLR4*$^{-/-}$ double knockout mice, endothelial-targeting lentiviral silencing constructs, and endothelial-targeted *Stat3*$^{-/-}$ mice to specifically demonstrate that Nox3 induction is responsible for the pro-oxidant, proapoptotic phenotype of *TLR4*$^{-/-}$ mice. We also show that an endothelial Hsp70-TLR4-Trif-Stat3 axis is required to suppress deleterious Nox3 induction. ***Innovation:*** To date, a physiologic role for Nox3 in oxidant-induced ALI has not been identified. In addition, we generated unique double knockout mice and endothelial-targeted lentiviral silencing constructs to specifically demonstrate the role of a TLR4 signaling pathway in regulating pro-oxidant generation. ***Conclusions:*** We identified an endothelial TLR4-Trif antioxidant pathway that leads to the inhibition of a novel NADPH oxidase, Nox3, in lungs and lung endothelial cells. We also identified the role of a TLR4 ligand, Hsp70, in suppressing Nox3 in basal and pro-oxidant conditions. These studies identify potentially new therapeutic targets in oxidant-induced ALI. *Antioxid. Redox Signal.* 24, 991–1012.

Introduction

DELIVERY OF HIGH LEVELS of inspired oxygen, or hyperoxia, is commonly used as a life-sustaining measure in critically ill patients. However, prolonged exposures can exacerbate respiratory failure and contribute to increased mortality. Hyperoxia also serves as a model for oxidant-mediated acute lung injury (ALI). The lungs are exposed continuously to oxidants generated either endogenously from phagocytes or exogenously from inhaled oxygen, as well as environmental pollutants. In addition, intracellular oxidants, such as those derived from the NADPH oxidase (Nox) system, are involved in many cellular signaling pathways.

There are seven isoforms of NADPH oxidases expressed in mammals: Nox1, Nox2, Nox3, Nox4, Nox5, Duox1, and Duox2 (13). Nox3 is the least described member of the Nox family. After its original cloning and detection in inner ear and fetal tissues, reports remain limited and its physiologic function thought to be limited to gravity perception (5, 19). We unexpectedly detected increased Nox3 expression, but not the alternative Noxs in the lungs of Toll-like receptor 4-deficient (*TLR4*$^{-/-}$) mice, which exhibited increased oxidant production and oxidant-mediated lung destruction (33). Consistent with our report of the pro-oxidant phenotype associated with TLR4 deficiency, *TLR4*$^{-/-}$ mice are also hypersusceptible to hyperoxia-induced ALI and death (35).

Recently, we found that the protective effect of TLR4 is related to its role in the lung structural cells, specifically lung endothelial TLR4 is required to resist lethal hyperoxia (28). However, the mechanisms whereby TLR4 deficiency leads to

[1]Section of Pulmonary, Critical Care and Sleep Medicine, Yale University School of Medicine, New Haven, Connecticut.
[2]Department of Pathology, Yale University School of Medicine and VA Connecticut Healthcare System, New Haven, Connecticut.

Innovation

Acute lung injury (ALI) is a major cause of morbidity and mortality, yet specific therapies do not exist. Excessive oxidant injury, from both endogenous and exogenous sources, is a key driver of ALI and ALI-associated organ failure. We identified an endogenous, novel immune pathway in the lungs and endothelium that protects against ALI and death. Our studies identify new molecular targets as well as endothelial-targeted approaches as potential new therapies against ALI.

an increased susceptibility to hyperoxia-induced ALI and death were unknown.

We generated *Nox3*$^{-/-}$/*TLR4*$^{-/-}$ double knockout mice, which exhibited less lung injury and death compared with *TLR4*$^{-/-}$ mice and identified a novel signaling axis, in which the endogenous TLR4 ligand, heat shock protein 70 (Hsp70), is required to inhibit Nox3 induction in lungs and endothelial cells *via* a TLR4-Trif (TIR domain-containing adapter-inducing interferon-β)-Stat3 (Signal transducer and activator of transcription 3) pathway. Furthermore, we overexpressed Nox3 in the lung and specifically targeted lung endothelial TLR4, Hsp70, and Stat3 *in vivo* using lentiviral constructs and endothelial-targeted knockout mice to provide proof of concept that the critical tissue compartment involved in the protective signaling is the lung endothelium. These studies identify new molecular targets as well as cell-specific approaches as therapy in patients with ALI.

Results

Nox3 deficiency rescues TLR4$^{-/-}$ *mice from lethal hyperoxia*

During our investigations of lung-protective molecules during hyperoxia, we identified that specific heat shock proteins signaled *via* TLR4. We were interested in determining the lung consequences of TLR4 deficiency during sterile oxidant stress, which led to our previous report of *TLR4*$^{-/-}$ mice having increased susceptibility to hyperoxia-induced ALI and death (35). We found that TLR4 messenger RNA (mRNA) and protein expression are upregulated during the first 72 h of hyperoxia in mouse lung endothelial cells (MLECs) and whole lung lysates (35) (Supplementary Fig. S1A; Supplementary Data are available online at www.liebertpub.com/ars). However, TLR4 expression declined by 96 h of hyperoxia, which coincides with maximal cell injury, as measured by lactate dehydrogenase (LDH) release, and inflammation, as measured by interleukin (IL)-6 release (Supplementary Fig. S1B–D).

We also reported that *TLR4*$^{-/-}$ mice showed Nox3 induction in mouse lungs and MLECs under basal conditions (33). To determine the *in vivo* role of Nox3 induction during hyperoxia, we generated *Nox3*$^{-/-}$/*TLR4*$^{-/-}$ double knockout mice and compared them with *Nox3*$^{-/-}$ and *TLR4*$^{-/-}$ mice under hyperoxia exposure. We first tested the impact of Nox3 on survival in wild-type (WT), *Nox3*$^{-/-}$, *TLR4*$^{-/-}$, and *Nox3*$^{-/-}$/*TLR4*$^{-/-}$ mice during hyperoxia challenge. *TLR4*$^{-/-}$ mice were significantly more susceptible to hyperoxia than WT mice, but in the absence of the Nox3, as shown by the *Nox3*$^{-/-}$/*TLR4*$^{-/-}$, their survival reverted to that of WT mice (Fig. 1A). Hyperoxia caused a significant increase in bronchoalveolar lavage (BAL) total cell counts, which consisted of macrophages, lymphocytes, and neutrophils, but not eosinophils in all four mouse strains (Fig. 1B–F). *TLR4*$^{-/-}$ mice had substantially more BAL macrophages, lymphocytes, and particularly neutrophils after hyperoxia compared with the BAL from WT and *Nox3*$^{-/-}$ mice after hyperoxia.

The *Nox3*$^{-/-}$/*TLR4*$^{-/-}$ double knockouts exhibited less BAL inflammatory cell recruitment compared with *TLR4*$^{-/-}$ mice, suggesting that Nox3 may be mediating, at least in part, the proinflammatory profile of *TLR4*$^{-/-}$ mice. We also checked other injury and oxidant markers such as BAL protein content, LDH, H_2O_2 production in BAL, and lipid peroxidation level in lung tissues (Fig. 1G–J). *Nox3*$^{-/-}$ mice had less injury after hyperoxia compared with WT and *TLR4*$^{-/-}$ mice. In addition, *Nox3*$^{-/-}$ mice had less lung inflammation and vascular leak, as assessed by BAL cell counts and BAL protein content, respectively, and oxidant production than WT mice (Fig. 1B–J). We quantitated apoptosis in lung tissue sections using terminal deoxynucleotidyl transferase dUTP nick-end labeling (TUNEL) staining and found that Nox3 deficiency diminished hyperoxia-induced lung apoptosis in *TLR4*$^{-/-}$ mice (Fig. 1K).

We also checked the expression of inflammatory proteins, such as tumor necrosis factor-α (TNFα), IL-1β, and IL-6, and found a similar pattern (Supplementary Fig. S1E). These data indicated that Nox3 deficiency attenuated reactive oxygen species (ROS) generation both at baseline and during oxidant injury and rescued the injury induced by hyperoxia in WT and *TLR4*$^{-/-}$ mice.

Next, we determined the effect of Nox3 overexpression on the lungs *in vivo*. We generated lentiviral Nox3 and delivered the overexpression construct, lenti-Nox3, or its control, lenti-Ctrl, intranasally to mice. We confirmed robust Nox3 induction after lenti-Nox3 delivery in total lungs, blood vessels, alveolar, and large airway tissue (Supplementary Fig. S1F-G). Overexpression of Nox3 resulted in decreased total antioxidant activity, increased lipid peroxidation level, and apoptosis in lung tissues (Fig. 2A–C). Lenti-Nox3 also markedly increased Nox3 expression in cultured primary MLEC (Fig. 2D) as well as hyperoxia-induced MLEC apoptosis (Fig. 2E). We performed dihydroethidine (DHE) staining as a general measure of ROS levels in live cells.

As shown in Figure 2F, lenti-Nox3 induced increased DHE signal in WT at baseline and during hyperoxia compared with lenti-Ctrl, confirming that lenti-Nox3 had a physiologic effect on primary cells. As expected, *TLR4*$^{-/-}$ MLECs had increased basal and hyperoxia-induced DHE staining (Fig. 2G). To identify whether the source of DHE staining was due to superoxide or NADPH oxidase, we treated *TLR4*$^{-/-}$ MLECs with superoxide dismutase (SOD) or an NADPH oxidase inhibitor, diphenylene iodonium (DPI), and found that both ablated DHE staining (Fig. 2G). These data suggested that there were likely more than one type and source for the increased ROS detected in *TLR4*$^{-/-}$ MLECs during basal and hyperoxic conditions.

Nox3 mediates, in part, oxidant generation and apoptosis in Hsp70$^{-/-}$ *and* TLR4$^{-/-}$ *MLECs*

Next, we were interested in identifying the signaling mechanisms whereby TLR4 inhibits Nox3 in lungs and MLECs. We had recently identified Hsp70 as an endogenous TLR4 ligand in lung tissue and MLECs, which exerts

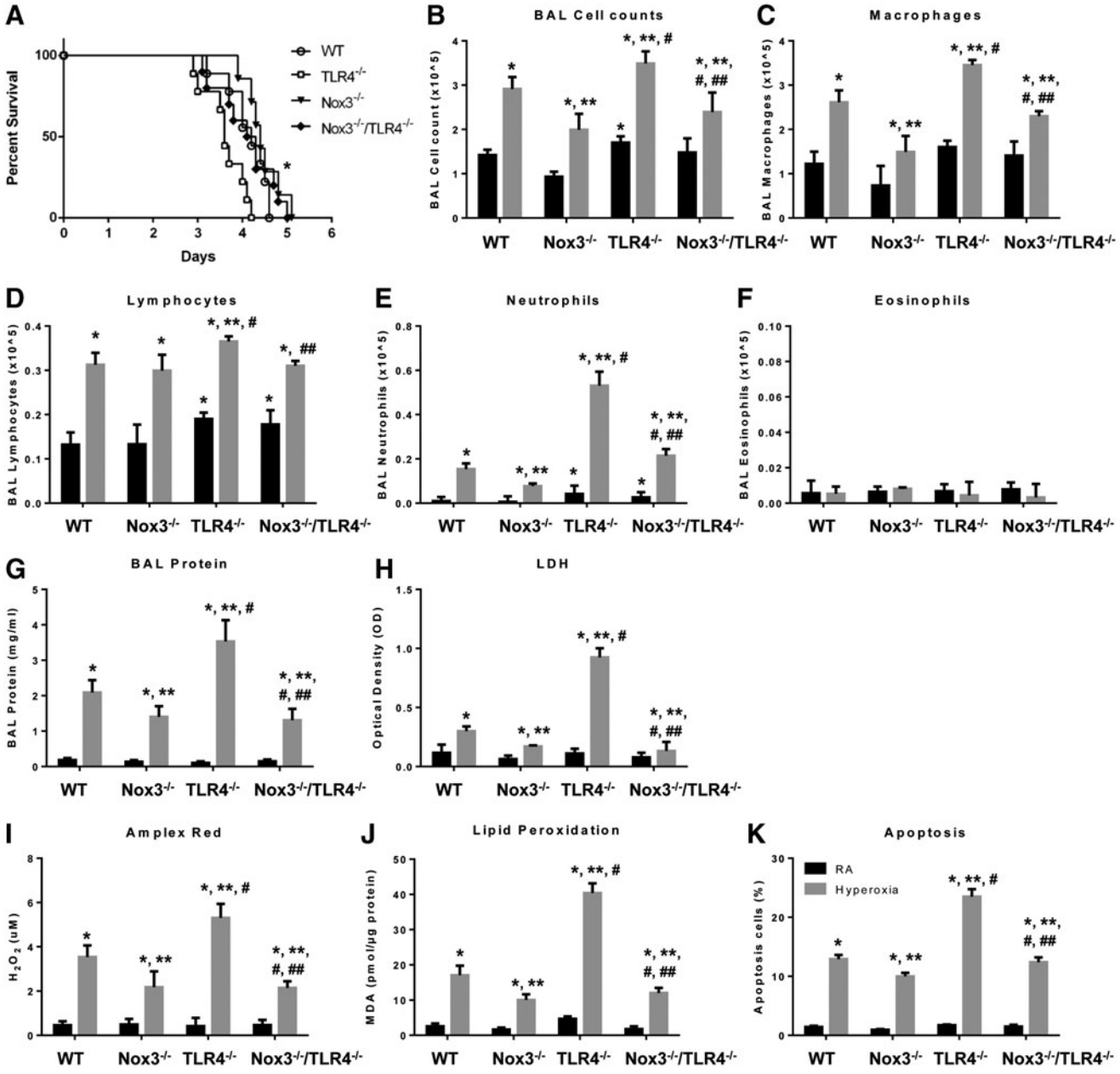

FIG. 1. Nox3 deficiency rescues *TLR4*$^{-/-}$ mice. (A) Survival proportions were compared among WT, *Nox3*$^{-/-}$, *TLR4*$^{-/-}$, and *Nox3*$^{-/-}$/*TLR4*$^{-/-}$ mice exposed to continuous hyperoxia ($n = 10$ for each group). $^{*}p < 0.01$ *versus TLR4*$^{-/-}$ mice. **(B–K)** Mice were exposed to RA or to hyperoxia for 72 h. Cells recovered from BAL were counted as BAL total cell counts **(B)**. Cytospins were prepared and the following cell populations were counted: macrophages **(C)**, lymphocytes **(D)**, neutrophils **(E)**, and eosinophils **(F)**. **(G)** Lung permeability was assessed by BAL protein content. **(H)** LDH activity assays were performed on BAL fluid. **(I)** Oxidant generation was detected by Amplex Red from BAL fluid. **(J)** MDA levels were measured in lung tissues using TBARS assay. **(K)** TUNEL-positive cells were quantitated and expressed as a percentage of the total number of lung cells counted on each section. The values are expressed as mean ± SD and analyzed by Mann–Whitney test ($n = 12$ for each group). $^{*}p < 0.05$ *versus* WT RA; $^{**}p < 0.05$ *versus* WT hyperoxia; $^{\#}p < 0.05$ *versus Nox3*$^{-/-}$ hyperoxia; $^{\#\#}p < 0.05$ *versus TLR4*$^{-/-}$ hyperoxia. BAL, bronchoalveolar lavage; LDH, lactate dehydrogenase; MDA, malondialdehyde; Nox, NADPH oxidase; RA, room air control; SD, standard deviation; TBARS, thiobarbituric acid-reactive substance; TLR4, Toll-like receptor 4; TUNEL, terminal deoxynucleotidyl transferase dUTP nick-end labeling; WT, wild-type.

significant lung protection against lethal hyperoxic injury (38). Hsp90 is known to regulate both TLR4 and Stat3, but we did not detect significant changes in Hsp90 expression after hyperoxia (Supplementary Fig. S1A).

We were interested in identifying potential links among TLR4-Hsp70 and Nox3. Given that we reported TLR4 adapter protein Trif, but not MyD88, to be involved in Hsp70 signaling, we used *Trif*$^{-/-}$ and *MyD88*$^{-/-}$ mice as additional controls.

We checked Nox3 expression and localization in mouse lungs using immunohistochemical staining and found low basal Nox3 expression in WT, but increased basal staining diffusely, especially in the airways and blood vessels of

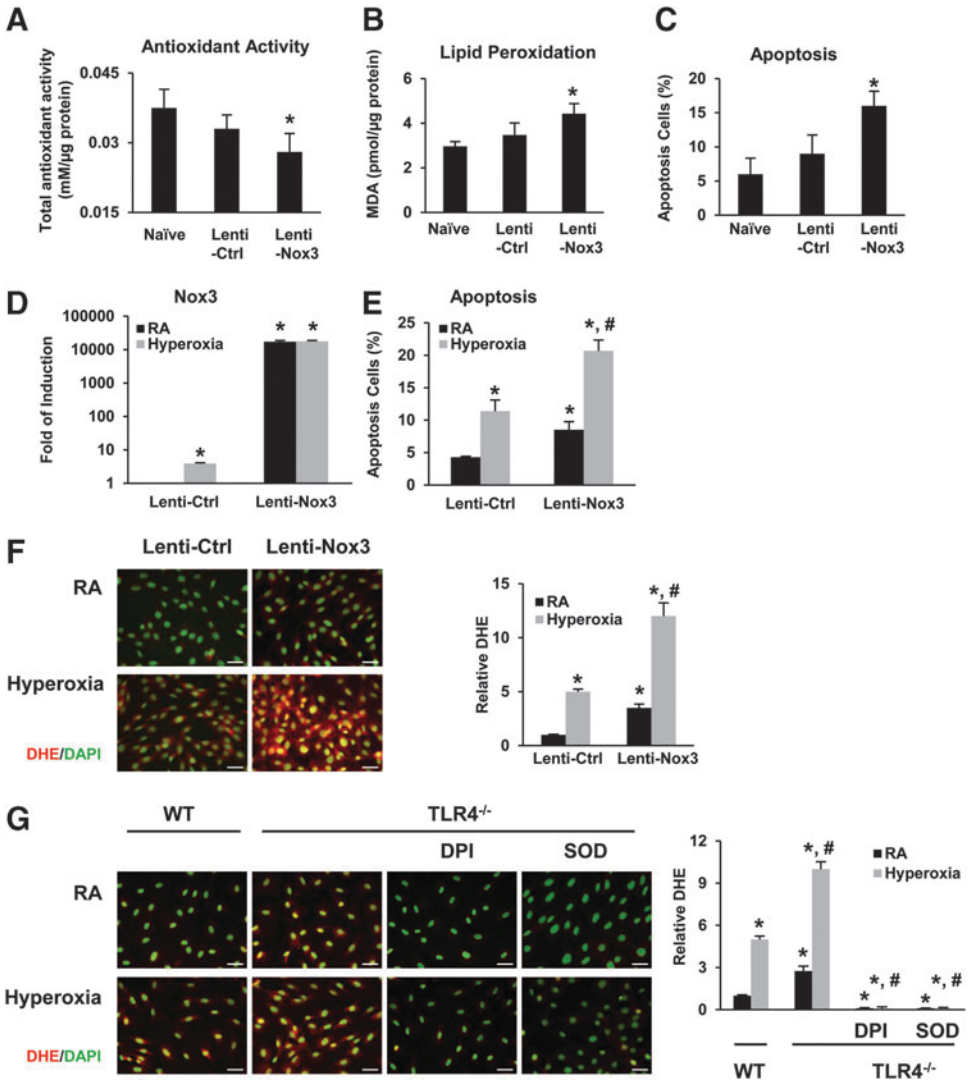

FIG. 2. Decreased antioxidant capacity and increased oxidant burden after Nox3 overexpression in mice and MLECs. **(A–C)** WT mice were administered intranasal lentivirus (lenti-Ctrl or lenti-Nox3); after 2 weeks, whole lung tissues were processed. **(A)** Total antioxidant activity was measured in the lung tissues. **(B)** MDA levels were measured in lung tissues using TBARS assay. **(C)** TUNEL staining was performed on lung sections and TUNEL-positive cells were quantitated and expressed as a percentage of the total number of lung cells counted on each section. The values are expressed as mean ± SD and analyzed by Mann–Whitney test ($n = 6$ for each group). *$p < 0.05$ *versus* lenti-Ctrl. **(D–F)** WT MLECs were infected with lentivirus (lenti-Nox3 or lenti-Ctrl), exposed to 72 h of hyperoxia, and the following performed: Nox3 mRNA expression **(D)**, graphical quantitation of flow cytometry analysis of apoptosis **(E)**, and DHE staining and relative DHE quantitation **(F)**. The values are expressed as mean ± SD and analyzed by Mann–Whitney test ($n = 6$ in each group). Images are representative of three independent experiments. At least 20 images per group were analyzed for quantification. Scale bar = 100 μm. *$p < 0.05$ *versus* lenti-Ctrl RA; #$p < 0.05$ *versus* lenti-Ctrl hyperoxia. **(G)** WT and *TLR4*$^{-/-}$ MLECs were exposed to 72 h of hyperoxia. DHE staining in the absence or presence of SOD (600 U/ml) or DPI (10 *μM*). Staining was analyzed with fluorescence microscopy and quantified using ImageJ. Images are representative of five independent experiments. Scale bar = 100 μm. The relative DHE values are expressed as mean ± SD and analyzed by Mann–Whitney test. *$p < 0.05$ *versus* WT RA; #$p < 0.05$ *versus* WT hyperoxia. DHE, dihydroethidine; DPI, diphenylene iodonium; MLEC, mouse lung endothelial cell; mRNA, messenger RNA; SOD, superoxide dismutase. To see this illustration in color, the reader is referred to the web version of this article at www.liebertpub.com/ars

TLR4$^{-/-}$, *Trif*$^{-/-}$, and *Hsp70*$^{-/-}$ mice, as detected by red cytoplasmic staining (Fig. 3A). Hyperoxia diffusely increased Nox3 staining in the lungs of both WT and *TLR4*$^{-/-}$ mice, but hyperoxia induction was greater in *TLR4*$^{-/-}$ (Supplementary Fig. S2A, B). Overexpression of Hsp70 using intranasal adenoviral Hsp70 (Ad-Hsp70) decreased Nox3 expression in WT mice in both basal and hyperoxia conditions, but Ad-Hsp70 had no effects on *TLR4*$^{-/-}$ mice (Fig. 3B), which supported our hypothesis that TLR4 is necessary for Hsp70-related Nox3 inhibition. We confirmed that Hsp70 deficiency recapitulated the Nox3 induction found in *TLR4*$^{-/-}$ lungs and MLECs by measuring Nox3 protein expression in *Hsp70*$^{-/-}$ MLECs (Fig. 3C).

We found that Nox3 mRNA expression was induced in both *TLR4*$^{-/-}$ and *Hsp70*$^{-/-}$ MLECs at baseline and after hyperoxia (Fig. 3D, Bars 5 and 7 *vs.* Bars 9 and 11). We also confirmed

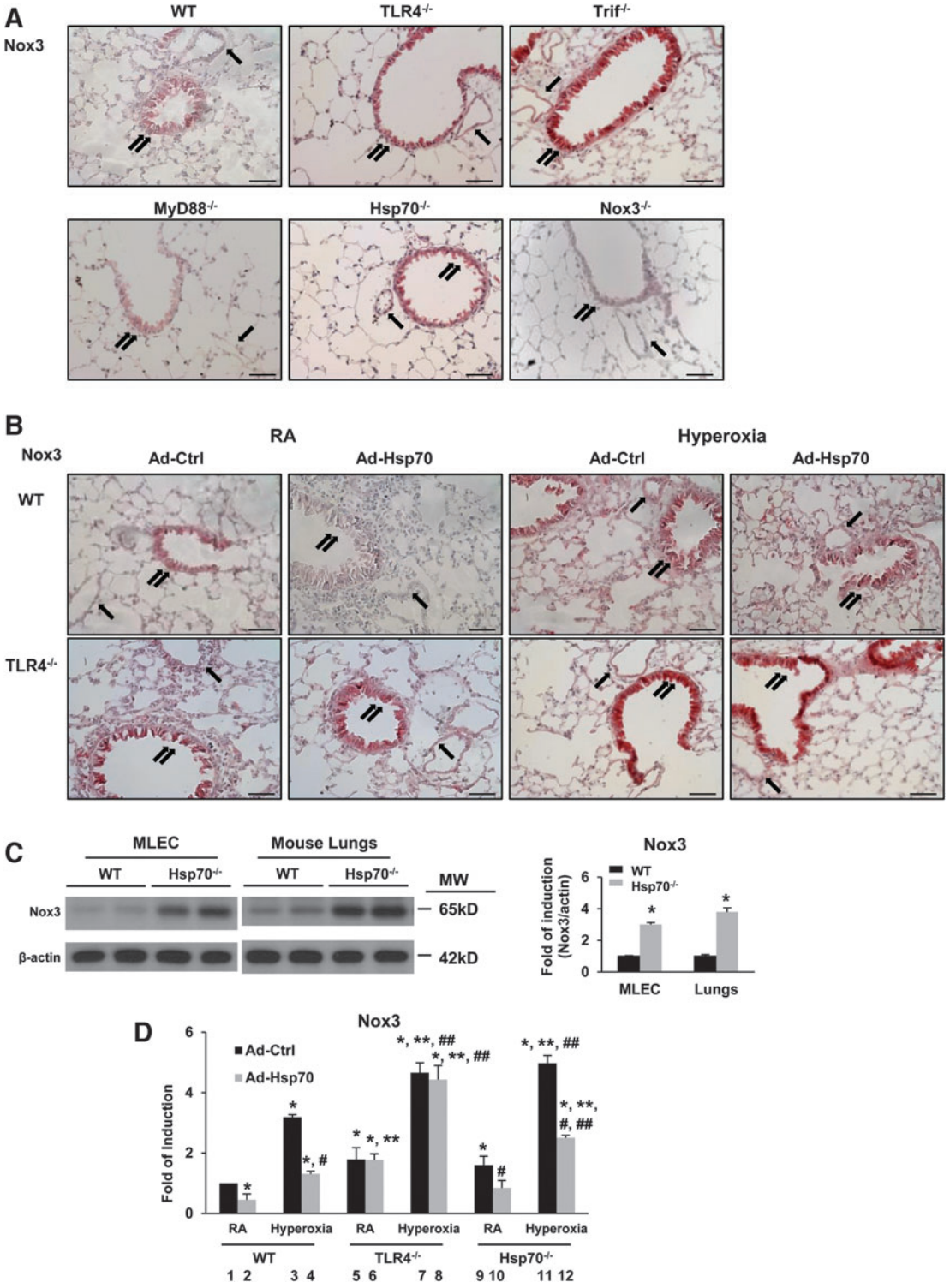

FIG. 3. TLR4-Hsp70 deficiency increases Nox3 protein expression in mouse lungs and MLECs. (A) Nox3 expression in mouse lungs with immunohistochemical staining. Nox3 protein is detected as red cytoplasmic staining. **(B)** Nox3 expression in mice lungs. WT and *TLR4*$^{-/-}$ mice were treated with Ad-Ctrl or Ad-Hsp70 and were exposed to 72 h of hyperoxia. Images are representative of five mice in each group. Airway, *double arrows*; blood vessels, *single arrows*. Scale bar = 250 μm. Images are representative of three independent experiments. **(C)** Lysates from MLECs or mouse lungs were isolated and immunoblotted against Nox3 antibody. β-Actin was used as protein loading control. One representative Western blot of three independent experiments is shown. Quantification based on densitometry for Nox3 and β-actin is shown on the *right panel*. The values are expressed as mean ± SD and analyzed by Mann–Whitney test (experiments were performed in triplicate). *$p < 0.05$ *versus* WT. **(D)** Nox3 mRNA levels in WT, *TLR4*$^{-/-}$, and *Hsp70*$^{-/-}$ MLECs were treated with Ad-Ctrl or Ad-Hsp70 and were exposed to 72 h of hyperoxia. The values are expressed as mean ± SD and analyzed by Mann–Whitney test (experiments were performed in triplicate). *$p < 0.05$ *versus* WT Ad-Ctrl RA; **$p < 0.05$ *versus* corresponding WT; $^{\#}p < 0.05$ *versus* corresponding Ctrl; $^{\#\#}p < 0.05$ *versus* corresponding RA. Ad-Ctrl, adenovirus control (CMV-null); Ad-Hsp70, adenoviral-Hsp70; Hsp70, heat shock protein 70. To see this illustration in color, the reader is referred to the web version of this article at www.liebertpub.com/ars

that Ad-Hsp70 is able to suppress Nox3 in WT MLECs and *Hsp70*$^{-/-}$, but not in *TLR4*$^{-/-}$, MLECs (Fig. 3D, Bars 12 *vs.* 8.). Basal Nox1, –2, and –4 expression levels were similar between WT and *TLR4*$^{-/-}$ lungs (33). There were also no differences in Nox1, –2, and –4 expression among WT, *TLR4*$^{-/-}$, and *Hsp70*$^{-/-}$ MLECs after hyperoxia (Supplementary Fig. S2C). These results suggested that inhibition of Nox3 expression is dependent on an Hsp70-TLR4 axis in lungs and MLECs.

Next, we wanted to determine the ability of TLR4 to specifically regulate Nox3 in lungs *versus* lung endothelium *in vivo*. We recently reported the efficiency and specificity of our TLR4 lentiviral constructs (28). We achieved total lung- and endothelial-TLR4 silencing, using lenti-TLR4sh or lenti-VE TLR4sh, respectively (Fig. 4A–C). WT mice, 2 weeks postintranasal administration of lentivirus, were exposed to 100% continuous oxygen for 72 h. Mice that received TLR4 silencing had significantly induced Nox3 expression compared with lenti-Ctrl mice before and after hyperoxia (Fig. 4A).

To confirm the cell-type specificity of our endothelial-targeted TLR4 silencer (lenti-VE TLR4sh) on Nox3

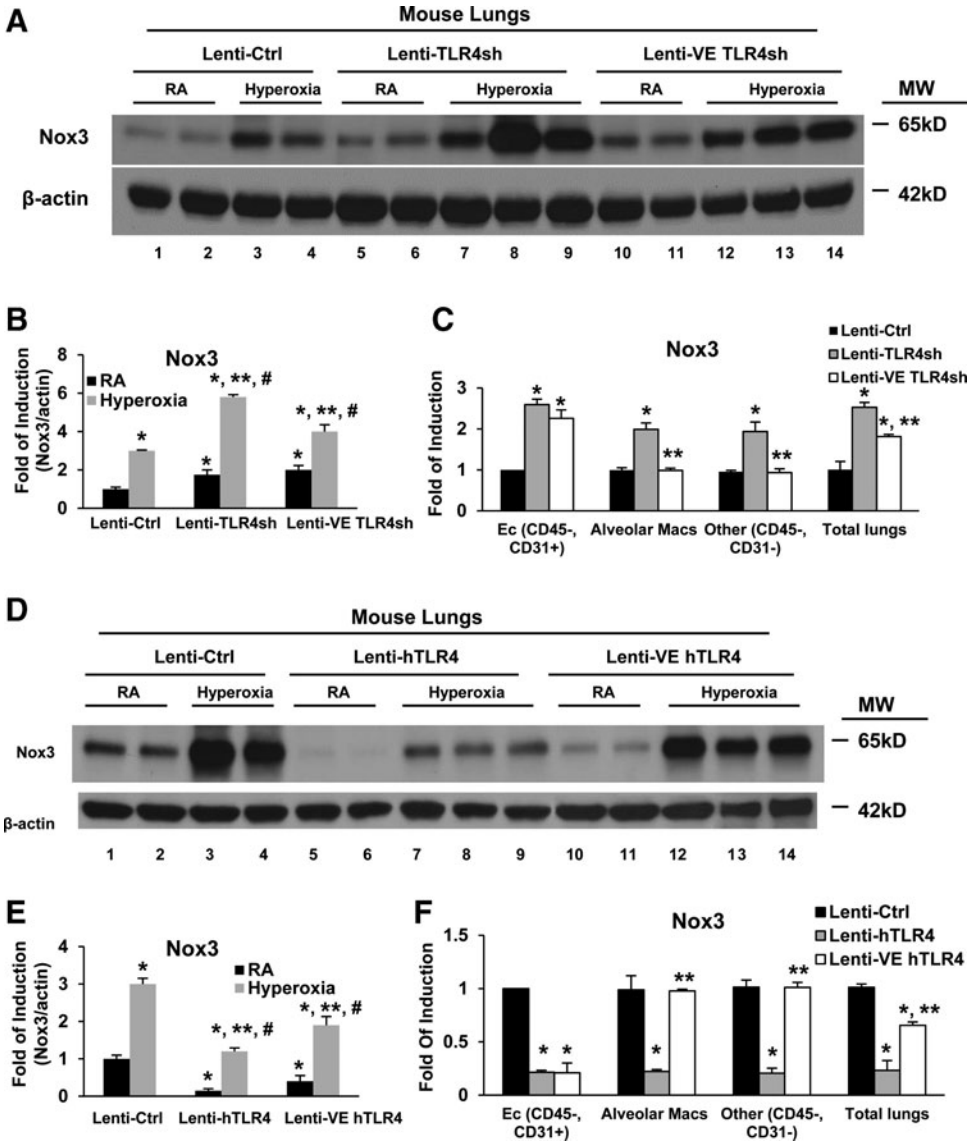

FIG. 4. TLR4 regulates Nox3 expression. WT mice were administered intranasal TLR4 silencers, lentivirus (lenti-Ctrl, lenti-TLR4sh, or lenti-VE TLR4sh) **(A–C)** or human TLR4 overexpressors, lentivirus (lenti-Ctrl, lenti hTLR4, or lenti-VE hTLR4) **(D–F)**, and exposed to RA or 72 h of hyperoxia. Lysates from mouse lungs were isolated and immunoblotted against antibodies as listed. β-Actin was used as protein loading control. One representative Western blot of three experiments is shown **(A, D)**. Quantification based on densitometry for Nox3 and β-actin is shown **(B, E)**. The values are expressed as mean ± SD and analyzed by Mann–Whitney test. Experiments were performed in triplicate.*$p < 0.05$ *versus* lenti-Ctrl RA; **$p < 0.05$ *versus* lenti-Ctrl hyperoxia; $^{\#}p < 0.05$ *versus* corresponding RA. **(C, F)** Nox3 expression was measured by qRT-PCR in endothelial cells ($CD45^-$, $CD31^+$), alveolar macrophages (obtained from BAL), double negative cells ($CD45^-$, $CD31^-$, which consist of epithelial, fibroblast, and smooth muscle cells), and whole lung tissue lysates. Nox3 mRNA levels are expressed as fold induction, which was calculated from $2^{-\Delta\Delta Ct}$ of mice that received lenti-TLR4sh or lenti-hTLR4 divided by the $2^{-\Delta\Delta Ct}$ of mice that received lenti-Ctrl. The values are expressed as mean ± SD and analyzed by Mann–Whitney test ($n = 4$ in each group). *$p < 0.05$ *versus* lenti-Ctrl; **$p < 0.05$ *versus* lenti-TLR4sh **(C)** or lenti-hTLR4 **(F)**. qRT-PCR, quantitative reverse transcription–polymerase chain reaction; sh, short hairpin.

induction, we delivered lenti-Ctrl, lenti-TLR4sh (a ubiquitious nonspecific promoter that should target all cells), and lenti-VE TLR4sh intranasally and then isolated endothelial cells ($CD45^-$, $CD31^+$), alveolar macrophages, and double negative cells ($CD45^-$, $CD31^-$, containing epithelial and smooth muscle cells) (Fig. 4C). Endothelium-specific silencing of TLR4, with lenti-VE TLR4sh, caused the greatest Nox3 induction in endothelial cells, whereas the nonspecific TLR4 silencer, lenti-TLR4sh, induced Nox3 in all cell types tested. As expected, both constructs induced Nox3 in total lungs given that lungs are comprised of ~40% endothelial cells.

We also performed TLR4 overexpression experiments using lentiviral-driven human TLR4 constructs that target all lung cells or endothelium, lenti-hTLR4, and lenti-VE hTLR4, respectively. We found that all lung- or endothelial-targeted TLR4 overexpression can inhibit both basal and hyperoxia-induced Nox3 expression in WT lungs (Fig. 4D, E). We again confirmed endothelial specificity of lenti-VE hTLR4 by sorting different cell types from total lung digests and determining that lenti-VE hTLR4 effectively inhibited basal Nox3 expression in the endothelium, but not in other cell types, whereas the nonspecific, all cell TLR4 overexpression construct was effective in all cell types tested (Fig. 4F). Taken together, these studies show that Nox3 induction is regulated by TLR4, including in the endothelium, and mediates lethal, pro-oxidant lung injury.

To determine the physiologic role of Nox3 specifically in *Hsp70*$^{-/-}$ and *TLR4*$^{-/-}$ MLECs, we performed gain-of-function and loss-of-function studies using Ad-Hsp70 and small interfering RNAs (siRNAs). Ad-Hsp70 decreased hyperoxia-induced oxidant production, as measured by DHE staining, in WT and *Hsp70*$^{-/-}$ MLECs, but not in *TLR4*$^{-/-}$ MLECs (Fig. 5A). Knockdown Nox3 by Nox3 siRNA in WT and *TLR4*$^{-/-}$ MLECs showed decreased hyperoxia-induced apoptosis (Fig. 5B). Nox3 siRNA also decreased oxidant generation induced by hyperoxia exposure compared with Ctrl siRNA (Fig. 5C). To determine whether Nox3 mediated Hsp70 deficiency-induced oxidant generation during hyperoxia, we generated double knockout mice (*Nox3*$^{-/-}$/*Hsp70*$^{-/-}$) and isolated the MLECs from this strain of mice. As expected, *Nox3*$^{-/-}$/*Hsp70*$^{-/-}$ MLECs had much less hyperoxia-induced apoptosis and oxidant generation compared with *Hsp70*$^{-/-}$ MLECs. *Nox3*$^{-/-}$ MLECs had similar much less hyperoxia-induced apoptosis and oxidant generation compared with WT MLECs. (Fig. 5D, E).

Furthermore, overexpression of Hsp70, using Ad-Hsp70, significantly decreased hyperoxia-induced oxidative stress (total ROS) and superoxide in WT and *Hsp70*$^{-/-}$ MLECs, but not in *TLR4*$^{-/-}$ MLECs, as measured by ROS/superoxide detection mix (Fig. 6A). Treatment with 5 m*M* N-acetylcysteine (NAC, ROS scavenger) also significantly reduced levels of total oxidative stress and superoxide. Pyocyanin (Pyo, 200 μM), an ROS inducer, served as a positive control (Fig. 6A). We also compared hyperoxia-induced total oxidative stress and superoxide generation among WT, *Nox3*$^{-/-}$, *TLR4*$^{-/-}$, *Nox3*$^{-/-}$/*TLR4*$^{-/-}$, *Hsp70*$^{-/-}$, and *Nox3*$^{-/-}$/*Hsp70*$^{-/-}$ MLECs (Fig. 6B). *Nox3*$^{-/-}$ MLECs exhibited lower basal and hyperoxia-induced total ROS and superoxide, whereas *TLR4*$^{-/-}$ and *Hsp70*$^{-/-}$ MLECs exhibited the highest.

If Nox3 were absent in *TLR4*$^{-/-}$ and *Hsp70*$^{-/-}$ MLECs, as achieved by generating double negative knockout MLECs, total ROS and superoxide levels were significantly decreased after hyperoxia. As a complementary approach, we also used a flow cytometry-based assay to detect hyperoxia-induced oxidative stress (total ROS) and superoxide in WT, *TLR4*$^{-/-}$, and *Nox3*$^{-/-}$ MLECs (Fig. 6C and Supplementary Fig. S2D).

We detected intracellular ROS generation in MLECs by measuring CM-H2DCFDA, an indicator of H_2O_2. We found that CM-H2DCFDA levels were significantly higher at baseline and after hyperoxia in *TLR4*$^{-/-}$ MLECs, which were not affected by Ad-Hsp70 due to the fact that Hsp70 requires TLR4 for antioxidant signaling. *Nox3*$^{-/-}$ MLECs had very low levels of basal and hyperoxia-induced CM-H2DCFDA (Fig. 6D, left panel).

Given that mitochondria are also a major source of ROS generation, we measured mitochondrial ROS in MLECs using MitoSOX Red, a fluorescent dye that detects mitochondrial ROS. Interestingly, we found that MitoSOX Red levels were significantly lower in *TLR4*$^{-/-}$ MLECs at baseline and after hyperoxia (Fig. 6D, right panel), the reasons for which will be explored in future studies. Ad-Hsp70 significantly inhibited hyperoxia-induced mitochondrial ROS in WT MLECs. *Nox3*$^{-/-}$ MLECs did not induce MitoSOX to the levels that WT MLECs did, but Ad-Hsp70 was still effective in blunting hyperoxia-induced mitochondrial ROS in *Nox3*$^{-/-}$.

Stat3 is required to inhibit Nox3 expression and mediate the protective effects of TLR4-Hsp70

Noxs are generally reported to be transcriptionally regulated, but the specific transcriptional factors involved remain poorly defined and virtually nothing is known about Nox3 regulation (15). We predicted that specific binding site analyses would help identify Nox3-regulating transcription factors, as has been reported for other Nox1 (29). Based on our previous report, in which endothelial Stat3 was essential for protective responses in oxidant-induced lung injury (34), we first used the Motif scan software (http://molbiol-tools.ca/Motifs.htm) to identify putative Stat binding sites (Statx) on the murine Nox3 gene promoter (Fig. 7A).

Using chromatin immunoprecipitation (ChIP) assays, we identified differentially bound Stat1/Stat3 on the Nox3 promoter in WT and *TLR4*$^{-/-}$ MLECs with or without Ad-Hsp70 (Fig. 7B). We found that regions −2534/−2360 and −1792/−1498 of the Nox3 promoter were critical binding sites for Stat3 in Hsp70-mediated Nox3 inhibition. We confirmed that lungs from endothelial Stat3-deficient (*Stat3*$^{E-/-}$) mice had more Nox3 expression at basal and after hyperoxia (Fig. 7C). MLECs isolated from *Stat3*$^{E-/-}$ mice had more basal as well as hyperoxia-induced Nox3 expression. Ad-Hsp70 decreased basal and hyperoxia-induced Nox3 expression, but it was dependent upon Stat3 (Fig. 9H). Ad-Hsp70 also decreased hyperoxia-induced injury, as assessed by LDH release (Fig. 7D), and apoptosis (Fig. 7E) in WT MLECs.

Next, we determined whether Stat3 was involved in TLR4-mediated resistance to hyperoxia-induced apoptosis. Stat3 siRNA treatment led to increased hyperoxia-induced apoptosis in MLECs (Fig. 7F). Overexpression of Stat3 by Ad-Stat3 had synergistic effects on Ad-Hsp70-mediated inhibition of apoptosis (Fig. 7G). We used complementary *in vitro* and *in vivo* approaches to specifically identify endothelial Stat3 as a necessary component of Nox3 inhibition and as a mediator of Hsp70-TLR4 protective signaling.

Stat3 suppressed Nox3 expression through an Hsp70-TLR4-Trif pathway in MLECs

Myd88 and Trif are the major adapter proteins for TLR4 signaling. We had previous data confirming that Hsp70 ameliorated hyperoxic injury *via* Trif, but not MyD88 *in vitro* and *in vivo* (36). Using electrophoretic mobility shift assays (EMSAs), we detected that Hsp70 induced Stat3 binding to the target sequence in WT and *MyD88*$^{-/-}$ MLECs, but not in *TLR4*$^{-/-}$ or *Trif*$^{-/-}$ MLECs (Fig. 8A). These results showed that Hsp70-mediated Stat3 activation and nuclear translocation were dependent on a TLR4-Trif pathway.

We proceeded to compare differences in specific signaling molecules downstream of TLR4 and upstream of Stat3 using WT, *TLR4*$^{-/-}$, *Trif*$^{-/-}$, and *MyD88*$^{-/-}$ MLECs with or without Ad-Hsp70 expression (Fig. 8B). We found that Hsp70 induced interferon regulatory factor 3 (IRF3) phosphorylation, interferon beta (IFNβ) expression, JAK1 phosphorylation, MEK phosphorylation, ERK1/2 phosphorylation, Stat3 activation (with Tyr 705 and Ser 727 phosphorylation), and, ultimately, suppression of Nox3 protein expression. We also analyzed other major kinase pathways involved in Tyr and Ser phosphorylation, such as p38-MKK3/6, JNK, and Tyk2 kinase, but we did not detect Ad-Hsp70-mediated differences (Supplementary Fig. S2E, F).

To confirm that the aforementioned signaling pathway was linked to Nox3, we compared the differences within key signaling factors that address our hypothesis in WT, *TLR4*$^{-/-}$, *Nox3*$^{-/-}$, and *Nox3*$^{-/-}$/*TLR4*$^{-/-}$ mice lung lysates (Fig. 8C). We found that *Nox3*$^{-/-}$/*TLR4*$^{-/-}$ mice had similar responses to hyperoxia in IRF3 phosphorylation, IFNβ expression, ERK1/2 phosphorylation, and Stat3 activation as *TLR4*$^{-/-}$ mice. Based on these results, we put forth a hypothesis of the signaling involved in Hsp70-TLR4-mediated suppression of Nox3 (Fig. 8D).

Signaling pathways involved in Hsp70-mediated Stat3 activation and Nox3 suppression

EMSA using IRF3 binding sites on the IFNβ promoter showed induction of IRF3 in WT and *MyD88*$^{-/-}$ MLECs, but not in *TLR4*$^{-/-}$ or *Trif*$^{-/-}$ MLECs treated with Ad-Hsp70 (Fig. 9A). Nox3 mRNA expression in WT and *TLR4*$^{-/-}$ MLECs was suppressed by IFNβ (10^3 unit/ml) treatment (Fig. 9B). IFNβ siRNA and the siRNA for its receptor, interferon alpha/beta receptor beta (IFNα/βRβ) siRNA, abolished the repression of Nox3 by Ad-Hsp70 (Fig. 9C, D). We also found that JAK1 inhibitor, piceatannol, MEK1/2 Inhibitor, U0126, and Erk inhibitor, A6355, abolished Ad-Hsp70-mediated activation of Stat3 and suppression of Nox3 expression (Fig. 9E–G). We confirmed our results using *Stat3*$^{-/-}$ MLECs (primary Ec from *Stat3*$^{E-/-}$ mouse lung), which exhibited less basal as well as hyperoxia-induced Hsp70 expression, ERK1/2 phosphorylation, and more Nox3 expression compared with WT MLECs (Fig. 9H).

Hsp70 activates Stat3 and suppresses Nox3 via *TLR4*

Next, we wanted to specifically invoke a role for endothelial Hsp70 in regulating Nox3 *in vivo*. Given that *Hsp70*$^{-/-}$ mice had increased mortality during hyperoxia (38), we used lung lysates from WT and *Hsp70*$^{-/-}$ mice lungs to confirm Hsp70-dependent Stat3 activation *in vivo* (Fig. 10A). As summarized in Figure 10B, hyperoxia activates Stat3 *via* MEK-ERK, leading to Hsp70 induction. Hsp70 then serves as a TLR4 ligand, which mediates IRF3-IFNβ activation. Hsp70 is likely involved in a feed-forward loop in which secreted Hsp70 activates Stat3, yet Hsp70 mediates its Nox3-inhibiting effects *via* Stat3. We assessed the impact of endothelial Hsp70 using lenti-VE Hsp70 short hairpin RNA (shRNA) and compared the results with that of total lung cell Hsp70 silencing using ubiquitin lenti-Hsp70 shRNA on Nox3 expression (Fig. 10C). Endothelial Hsp70 silencing was as effective as ubiquitous Hsp70 silencing, suggesting that endothelial Hsp70 is a major contributor to Nox3 inhibition *in vivo*.

Discussion

Oxygen therapy is a necessary and life-saving component in the treatment of critically ill patients, but prolonged oxygen therapy at high concentrations (hyperoxia) is sometimes necessary to maintain adequate tissue oxygenation. Unfortunately, hyperoxia can also exacerbate ALI and increase mortality. With recent advancements in oxygen delivery to

FIG. 5. Hsp70-TLR4 deficiency increases oxidants and apoptosis, in part *via* Nox3 induction, in MLECs. (A) DHE staining in WT, *TLR4*$^{-/-}$, and *Hsp70*$^{-/-}$ MLECs after treatment with Ad-Ctrl or Ad-Hsp70, which were then exposed to 72 h of hyperoxia. Staining was analyzed by fluorescence microscopy and quantified using ImageJ. Images are representative of five independent experiments. At least 20 images per group were analyzed for quantification. Scale bar = 100 μm. The relative DHE values are expressed as mean ± SD and analyzed by Mann–Whitney test. *$p < 0.05$ *versus* WT Ad-Ctrl RA; **$p < 0.05$ *versus* corresponding WT; $^{\#}p < 0.05$ *versus* corresponding Ctrl; $^{\#\#}p < 0.05$ *versus* corresponding RA. **(B)** WT and *TLR4*$^{-/-}$ MLECs were transfected with Nox3 siRNA and were treated with Ad-Ctrl or Ad-Hsp70, followed by exposure for 72 h of hyperoxia. Graphical quantitation of flow cytometry analysis of apoptosis. The values are expressed as mean ± SD and analyzed by Mann–Whitney test ($n = 5$ each group). *$p < 0.05$ *versus* corresponding Ctrl siRNA Ad-Ctrl RA group; **$p < 0.05$ *versus* corresponding Ad-Ctrl group; $^{\#}p < 0.05$ *versus* corresponding Ctrl siRNA group. **(C)** DHE staining in WT and *TLR4*$^{-/-}$ MLECs, which were transfected with Nox3 siRNA and exposed to 72 h of hyperoxia. Images are representative of five independent experiments. At least 20 images per group were analyzed for quantification. Scale bar = 100 μm. The relative DHE values are expressed as mean ± SD and analyzed by Mann–Whitney test. *$p < 0.05$ *versus* WT Ctrl siRNA RA; **$p < 0.05$ *versus TLR4*$^{-/-}$ Ctrl siRNA RA; $^{\#}p < 0.05$ *versus* WT Nox3 siRNA RA; $^{\#\#}p < 0.05$ *versus* corresponding WT. Graphical quantitation of flow cytometry analysis of apoptosis **(D)** or DHE staining and DHE quantitation **(E)** in WT, *Hsp70*$^{-/-}$, *Nox3*$^{-/-}$, and *Hsp70*$^{-/-}$/*Nox3*$^{-/-}$ MLECs, which were exposed to 72 h of hyperoxia. The values are expressed as mean ± SD and analyzed by Mann–Whitney test ($n = 5$ in each group). *$p < 0.05$ *versus* WT RA; **$p < 0.05$ *versus* WT hyperoxia; $^{\#}p < 0.05$ *versus* corresponding RA. Images are representative of five independent experiments. At least 20 images per group were analyzed for quantification. Scale bar = 100 μm. siRNA, small interfering RNA. To see this illustration in color, the reader is referred to the web version of this article at www.liebertpub.com/ars

patients with severe lung disease, using flow rates as high as 50 L per minute at 100% oxygen concentration, we are potentially putting our patients at increased risk for ALI, yet effective specific therapies for ALI do not exist.

Animal models of hyperoxia mimic major features of human ALI, such as pulmonary epithelial and endothelial cell death, increased pulmonary capillary permeability, inflammation, and eventually respiratory failure. Our current studies identify a novel, protective signaling cascade in lung endothelium, which has a significant impact on the outcome of hyperoxia-induced ALI and mortality.

We previously reported that lung-targeted activation of TLR4 confers resistance to hyperoxia-induced apoptosis (22). Although TLR4 is known to play critical roles in innate and adaptive immune responses, the role of cytoprotective TLR4 signaling in stromal cells, such as endothelium, is poorly understood. We also found that Hsp70 acts as a functional, endogenous TLR4 ligand during hyperoxia, which promotes endothelial cell survival *in vivo* and *in vitro* (38). We initially identified Nox3, but not the alternative Noxs, in TLR4-deficient lungs and cells, but *in vivo* consequences of Nox3 induction in the lung and its mechanism of regulation by TLR4

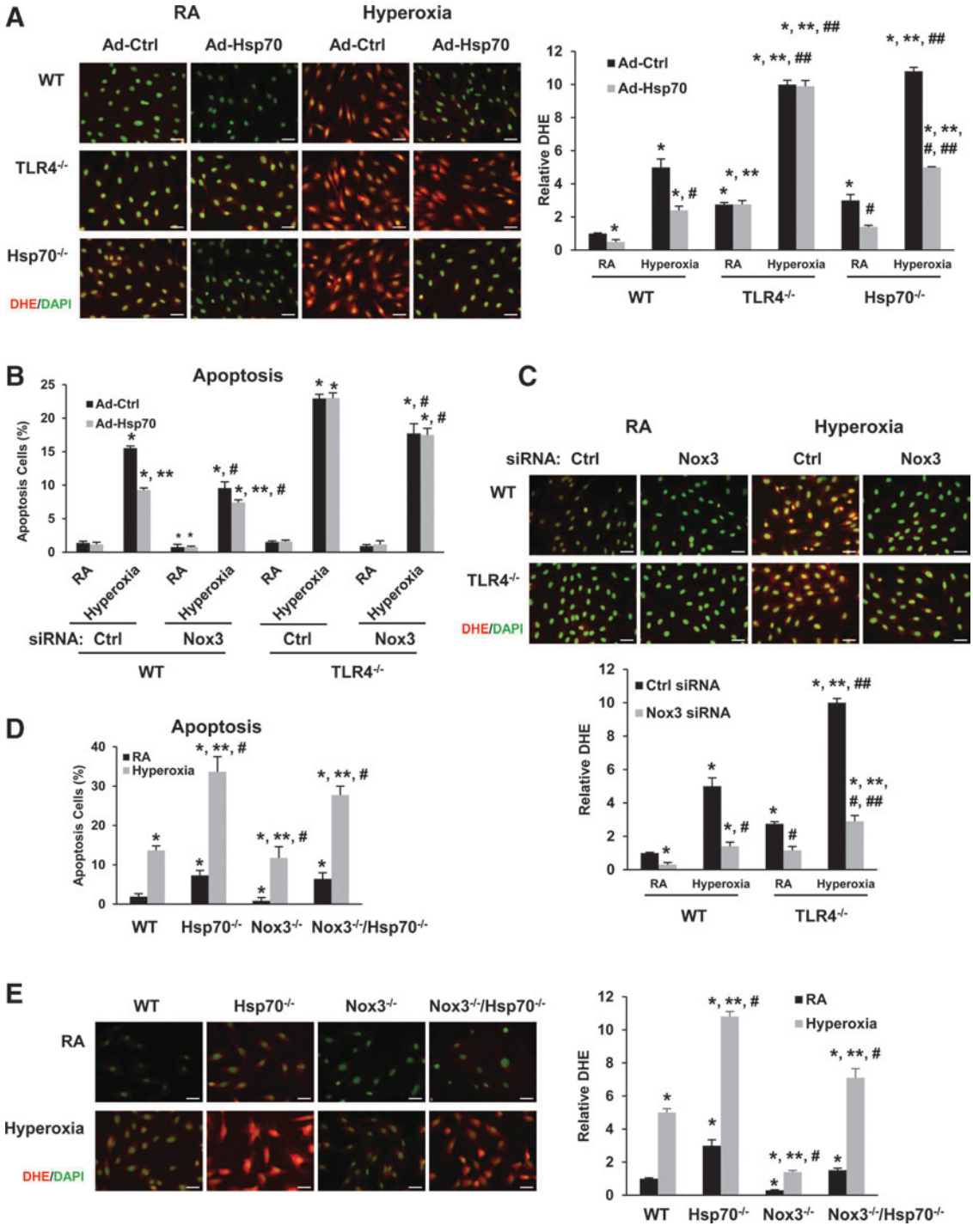

were unknown (33). In combination with the current studies, we present a new paradigm of an endogenous protective pathway in the endothelium, in which Hsp70 is induced and released as an adaptive stress response to hyperoxia and then, *via* TLR4-Trif-Stat3 activation, it can limit excessive oxidative stress by inhibiting the expression of Nox3.

Lentiviruses have the ability to infect both dividing and nondividing cells and integrate their genetic cargo directly into the chromosome of the target cell, but not transfer sequences that encode proteins derived from the packaging virus. However, limitations include size constraints for the insert, DNA methylation-induced promoter silencing, heterogeneously fluorescent toxicity, and insertional mutagenesis (7). In the current study, we used third-generation lentiviral vectors, which are designed to be self-inactivating and delete most of the viral genome, leaving room for transgenes and sequences of up to 8 kb in size.

We also detected high efficiency and specific targeting in endothelium and lung tissues. We did not observe overt cell toxicity when we tested EGFP as a transgenic tag to detect the short hairpin fragment targeting (36). We also reported that intranasal lentiviral delivery did not appear to have off-target organ distribution (28). However, both adenoviral and lentiviral constructs produce mild inflammation acutely in the lung. To minimize this side effect, we allow mice to recover for 2 weeks after viral delivery before proceeding with hyperoxia and always use empty lentivirus as a control (36–38). To confirm the specificity of our *in vivo* results, we perform parallel studies *in vitro* whenever possible.

In vitro siRNA studies are also limited by variability of transfection, incomplete knockdown, and the potential off-target effects as well. However, the combination of genetic, siRNA, and pharmacologic manipulations hopefully minimizes nonspecific effects due to the technical limitations of each of these approaches.

Nox activity is a principal source of phagocytic oxidant generation, yet its role in nonphagocytic cells is only recently emerging. Recently, several novel homologs of Nox2 have been described in a variety of nonphagocytic cells (Nox1-5 and Duox1-2) (9, 14).

Nox1 expression in tumor tissues was correlated with TLR4 expression and clinical stages in nonsmall cell lung cancer (NSCLC) patients and promoted tumor metastasis *via* TLR4 (16). Nox2-mediated endothelial eNOS-S-glutathionylation leads to uncoupled superoxide production and endothelial barrier dysfunction in ALI (31). Sanders *et al.* observed constitutively high levels of Nox4 expression and activity in cellular senescence of lung fibroblasts, thus implicating Noxs in age-related pathology (25). Although a direct interaction between TLR4 and Nox4 has been described in phagocytic cells (20), our studies are the first to link TLR4 with a novel Nox, Nox3, in the endothelium.

Nox expression is generally thought to be controlled at the level of gene transcription. Nox3 mRNA has been detected by reverse transcription–polymerase chain reaction (RT-PCR) in fetal kidney, liver, lung, and spleen (5). Recently, a functional role for Nox3 was reported within the inner ear (vestibular system), in which Nox3-derived oxidants were implicated in hearing loss and balance problems (1, 19). Nox3 is the predominant source of palmitate-induced ROS generation and is thought to drive palmitate-induced hepatic insulin resistance through JNK and p38 (MAPK) pathways (8). Nox3 also triggers spermatogonial stem cell self-renewal (18). Nox3 activation during ischemia–reperfusion injury may contribute to the development of primary graft dysfunction after lung transplantation (4).

In support of our previous report, in which we detected increased Nox3 in *TLR4*$^{-/-}$ mice, Ruwanpura *et al.* reported that elevated oxidative protein carbonylation levels and increased numbers of alveolar cell apoptosis were detected in *TLR4*$^{-/-}$ mice, along with upregulation of Nox3 mRNA expression (23). Our studies of double *TLR4*$^{-/-}$*/Nox3*$^{-/-}$ mice demonstrate for the first time *in vivo* that Nox3 mediates, at least in part, the lung injury phenotype of *TLR4*$^{-/-}$ mice.

Nox inhibition has been described to have therapeutic effects. Knockdown of Nox3 by pretreatment with siRNA

FIG. 6. Hsp70-TLR4 deficiency increases superoxide generation in MLECs. (A) WT, *TLR4*$^{-/-}$, and *Hsp70*$^{-/-}$ MLECs were treated with Ad-Ctrl or Ad-Hsp70 and then exposed to 72 h of hyperoxia. Cells were incubated with 1 μM ROS/Superoxide Detection Mix for 60 min at 37°C. WT MLECs were incubated with ROS inducer, pyocyanin (Pyo, 200 μM), or ROS inhibitor, N-acetyl-L-cysteine (NAC, 5 mM), as positive and negative controls, respectively. Changes in fluorescence intensity were measured using a fluorometer (SpectraMAX Gemini XS; Molecular Devices) at excitation/emission wavelengths of 488/520 nm (oxidative stress) and 550/610 nm (superoxide). The quantification of data for total ROS is shown in the *left panel* and superoxide quantification is shown in the *right panel*. Data are expressed as mean ± SD and analyzed by Mann–Whitney test ($n = 6$ in each group). $^{*}p < 0.05$ *versus* WT Ad-Ctrl RA; $^{**}p < 0.05$ *versus* WT Ad-Hsp70 RA; $^{\#}p < 0.05$ *versus* WT Ad-Ctrl hyperoxia; $^{\#\#}p < 0.05$ *versus* WT Ad-Hsp70 hyperoxia; $^{\$}p < 0.05$ *versus Hsp70*$^{-/-}$ Ad-Ctrl RA; $^{\$\$}p < 0.05$ *versus Hsp70*$^{-/-}$ hyperoxia. **(B)** Total ROS and superoxide were detected in WT, *Nox3*$^{-/-}$, *TLR4*$^{-/-}$, *Nox3*$^{-/-}$*/TLR4*$^{-/-}$, *Hsp70*$^{-/-}$, and *Nox3*$^{-/-}$*/Hsp70*$^{-/-}$ MLECs exposed to 72 h of hyperoxia. Data are expressed as mean ± SD and analyzed by Mann–Whitney test ($n = 6$ in each group). $^{*}p < 0.05$ *versus* WT RA; $^{**}p < 0.05$ *versus* WT hyperoxia; $^{\#}p < 0.05$ *versus* corresponding RA; $^{\#\#}p < 0.05$ *versus Nox3*$^{-/-}$ hyperoxia; $^{\$}p < 0.05$ *versus TLR4*$^{-/-}$ hyperoxia; $^{\$\$}p < 0.05$ *versus Hsp70*$^{-/-}$ hyperoxia. **(C)** Quantification of ROS-positive cells and superoxide-positive cells measured by flow cytometry. WT, *TLR4*$^{-/-}$, and *Nox3*$^{-/-}$ MLECs were exposed to 72 h of hyperoxia. Graphical quantitation of flow cytometry analysis and representative log FL1 (*x*-axis) *versus* log FL2 (*y*-axis) dot plots as shown in Supplementary Figure S2D. The values are expressed as the percentage of the total number of cells counted (mean ± SD and analyzed by Mann–Whitney test, $n = 6$ in each group). $^{*}p < 0.05$ *versus* WT RA; $^{**}p < 0.05$ *versus* WT hyperoxia; $^{\#}p < 0.05$ *versus* corresponding RA; $^{\$}p < 0.05$ *versus TLR4*$^{-/-}$ RA; $^{\$\$}p < 0.05$ *versus TLR4*$^{-/-}$ hyperoxia. **(D)** WT, *TLR4*$^{-/-}$, and *Nox3*$^{-/-}$ MLECs were treated with Ad-Ctrl or Ad-Hsp70 and were exposed to 72 h of hyperoxia. H_2O_2 generation was determined by CM-H2DCFDA (*left panel*) and mitochondrial ROS was determined by MitoSOX Red (*right panel*); levels were measured by flow cytometry. Values are expressed as mean ± SD and analyzed by Mann–Whitney test ($n = 6$ in each group). $^{*}p < 0.05$ *versus* WT Ad-Ctrl RA; $^{**}p < 0.05$ *versus* WT Ad-Hsp70 RA; $^{\#}p < 0.05$ *versus* WT Ad-Ctrl hyperoxia; $^{\#\#}p < 0.05$ *versus* WT Ad-Hsp70 hyperoxia; $^{\$}p < 0.05$ *versus Nox3*$^{-/-}$ Ad-Ctrl RA; $^{\$\$}p < 0.05$ *versus Nox3*$^{-/-}$ hyperoxia. ROS, reactive oxygen species.

prevented cisplatin ototoxicity, as demonstrated by preservation of hearing thresholds and inner ear sensory cells (24). Preventing Nox2 activation and the amplification of lung injury associated with inflammation can protect lungs against damage from hyperoxia (2). Genetic and pharmacological targeting of Nox4 in aged mice with established fibrosis attenuated the senescent, apoptotic-resistant myofibroblast phenotype and led to a reversal of fibrosis (10). To the best of our knowledge, our studies are the first to identify Nox3 as a therapeutic target in the lungs.

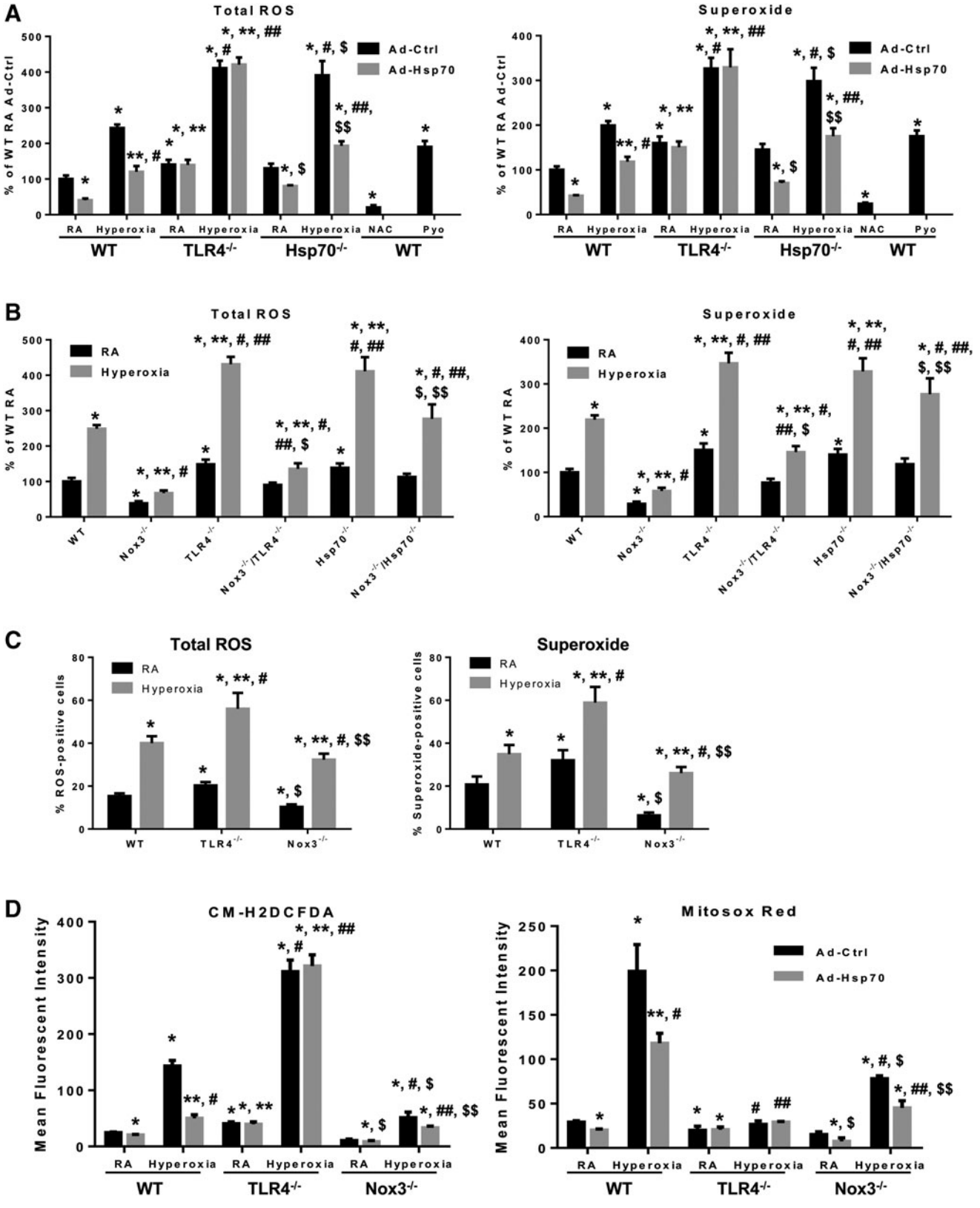

We envision specific Nox3 inhibitors as a preventative or therapeutic approach for sterile ALI or for pulmonary processes in which endothelial dysfunction and oxidant imbalance are key features, such as ALI and pulmonary hypertension. Recently, several new isoform-specific Nox inhibitors and biological peptidic inhibitors of Nox 1, Nox2, Nox 4, and Nox 5 have been identified (17) and similar strategies may be employed against Nox3.

The oxidant assays we employed to detect Nox3 activity are not highly specific for superoxide, the main ROS produced by all Noxs. Since superoxide has a very short life, it is difficult to detect as a dominant signaling intermediate. The efficacy of superoxide dismutation into H_2O_2 is affected by the abundance of intracellular SOD and small reducing molecules such as glutathione (3). There are a few methods to detect superoxide and its dismutation product (H_2O_2) directly and indirectly. DHE was originally considered to be a relatively specific method to detect intracellular and extracellular superoxide produced by NADPH oxidase (21), but it was also used to detect mitochondrial superoxide (27), $ONOO^-$, or $^{\bullet}OH$ (30).

New state-of-the-art methods to detect superoxide include new fluorescent probes, electron spin resonance approaches, and immunoassays, but there has been limited translation of some of methods, such as electron spin resonance, into biomedical research (6). In the absence of direct measurements using HPLC or electron spin, we selected a variety of indirect, but ideally complementary, assays such as DHE to check cytosolic superoxide; CM-H2DCFDA for intracellular H_2O_2, MitoSOX Red for mitochondrial superoxide, Amplex Red to check extracellular H_2O_2, and thiobarbituric acid-reactive substance (TBARS) assay for lipid peroxidation. We also confirmed our results with total ROS/superoxide detection systems for live cells by using microassays as well as flow cytometry-based methods. The results were remarkably consistent in terms of the pro-oxidant milieu that results from Hsp70-TLR4 deficiency or Nox3 induction.

We show that endothelial Hsp70-TLR4 signaling suppresses Nox3 and excessive oxidant production, which was sufficient to protect against lethal hyperoxia. Lung-targeted Nox3 overexpression also resulted in increased oxidative stress, lung injury, and cell death *in vivo*. We identified Stat3 binding sites on the Nox3 gene promoter and determined a functional role of Stat3 in Nox3 expression and in mitigating hyperoxia-induced cell death. We proceeded upstream of Stat3 and identified the relative contribution of TLR4 adapter proteins, MyD88 and Trif. We also generated *Nox3*$^{-/-}$/*TLR4*$^{-/-}$ double knockout mice, which showed significantly decreased hyperoxia-induced ALI compared with *TLR4*$^{-/-}$ mice. Furthermore, we demonstrated the utility of endothelial-targeting strategies *in vivo*, using genetic or intranasal lentiviral constructs, to invoke the critical role of the lung endothelium. These studies identify an Hsp70-TLR4-Trif-Nox3 axis in lung endothelium as potential therapeutic targets against hyperoxia-induced lung injury.

Materials and Methods

Mice

TLR4$^{-/-}$ mice (originally provided by S. Akira, Osaka University, Osaka, Japan) have been previously described (33). TLR4-deficient mouse lines, C3H/HeJ and C57BL/10ScNJ, and their respective controls were purchased from the Jackson Laboratory (Bar Harbor, ME). *Nox3*$^{-/-}$ mice ($Nox3^{het\text{-}4J}$) were purchased from Jackson Laboratory. Conditional endothelial-targeted Stat3-deficient mice (*Stat3*$^{E-/-}$) and their WT littermate controls have been described (12). In brief, two loxP sites were flanked into exons 18–20, the SH2 domain of Stat3. The Tie2e-Cre transgenic mouse strain was generated to express Cre under the control of the TIE2-kinase promoter/enhancer. The TIE2e-Cre;*Stat3*$^{f/d}$ mutant mice (*Stat3*$^{E-/-}$) were generated through TIE2e-Cre;$Stat3^{+/d}$ mice crossed with *STAT3*$^{f/f}$ mice (Stat3 WT). *Hsp70*$^{-/-}$, *Trif*$^{-/-}$, and *MyD88*$^{-/-}$ mice were described previously (11, 38), which simultaneously inactivate both Hsp70.1 and Hsp70.3 after homologous recombination. *Hsp70*$^{-/-}$, *Trif*$^{-/-}$, and *MyD88*$^{-/-}$ mice were described previously (11, 38). All the mice were backcrossed for >10 generations onto a C57BL/6J background. *Nox3*$^{-/-}$/*TLR4*$^{-/-}$ mice were generated by crossing *Nox3*$^{-/-}$ mice with *TLR4*$^{-/-}$ mice for >10 generations. *Nox3*$^{-/-}$/*Hsp70*$^{-/-}$mice were generated by crossing *Hsp70*$^{-/-}$

FIG. 7. Stat3 is required to inhibit Nox3 expression and mediate the protective effects of TLR4-Hsp70. (A) Putative Stat binding sites (Statx) on the murine Nox3 gene promoter. **(B)** WT and *TLR4*$^{-/-}$ MLECs treated with Ad-Ctrl or Ad-Hsp70. Electrophoretic profiles of the DNA products amplified in chromatin immunoprecipitation assay analysis at the Stat1 and Stat3 binding sites of Nox3. Quantification based on relative densitometry for PCR products is shown on the *right panel*. The values are expressed as mean ± SD and analyzed by Mann–Whitney test. Experiments were performed in triplicate. *$p < 0.05$ *versus* WT Ad-Ctrl. **(C)** WT and *Stat3*$^{E-/-}$ mice were exposed to 72 h of hyperoxia. Lung lysates were immunoblotted against Nox3 antibody. β-Actin was used as protein loading control. One representative Western blot of three experiments is shown. Quantification based on densitometry for Nox3 relative to β-actin is shown on the *right panel*. Experiments were performed in triplicate. The values are expressed as mean ± SD and analyzed by Mann–Whitney test ($n = 6$ for each group). *$p < 0.05$ *versus* WT RA; **$p < 0.05$ *versus* WT hyperoxia; $^{\#}p < 0.05$ *versus* corresponding RA. **(D, E)** WT and *Stat3*$^{-/-}$ MLECs were exposed to72 h of hyperoxia. $Stat3^{-/-}$ MLECs were isolated from endothelial-targeted Stat3-deficient mice (*Stat3*$^{E-/-}$), as described in the Materials and Methods section. **(D)** LDH activity assay from MLEC supernatant. **(E)** Quantitation of flow cytometry analysis of apoptosis. The values are expressed as mean ± SD and analyzed by Mann–Whitney test ($n = 6$ in each group). *$p < 0.05$ *versus* Stat3 WT Ad-Ctrl RA; **$p < 0.05$ *versus* Stat3 WT Ad-Ctrl hyperoxia; $^{\#}p < 0.05$ *versus* corresponding Ad-Ctrl. WT and *TLR4*$^{-/-}$ MLECs were transfected with Stat3 siRNA **(F)** or treated with Ad-Stat3 **(G)** and were treated with Ad-Hsp70, followed by exposure for 72 h of hyperoxia. Graphical quantitation of flow cytometry analysis of apoptosis. The values are expressed as mean ± SD and analyzed by Mann–Whitney test ($n = 6$ for each group). *$p < 0.05$ *versus* corresponding Ctrl siRNA **(F)** or no Ad-Stat3 **(G)** in RA Ad-Ctrl group; **$p < 0.05$ *versus* corresponding Ad-Ctrl group; $^{\#}p < 0.05$ *versus* corresponding Ctrl siRNA **(F)** or no Ad-Stat3 **(G)** group. Stat3, signal transducer and activator of transcription 3.

mice with *Nox3*$^{-/-}$ mice for >10 generations. Mice were bred and exposed to hyperoxic as described previously (36). All protocols were reviewed and approved by the Animal Care and Use Committee at Yale University.

Hyperoxia exposures

For hyperoxia experiments, mice were placed in a Plexiglas chamber with 5 L per minute of 100% oxygen using continuous flow (35). For survival experiments, mice were monitored closely and their survival in hours was recorded. Mice were allowed food and water *ad libitum*. For injury experiments, after 72 h [extreme injury, as described previously (26)] of hyperoxia exposure, mice were removed from the hyperoxia chamber and euthanized. Lung specimens were obtained for histology, RNA and protein extraction, apoptosis, and immunohistochemistry analyses as described below. All animal protocols were reviewed and approved by

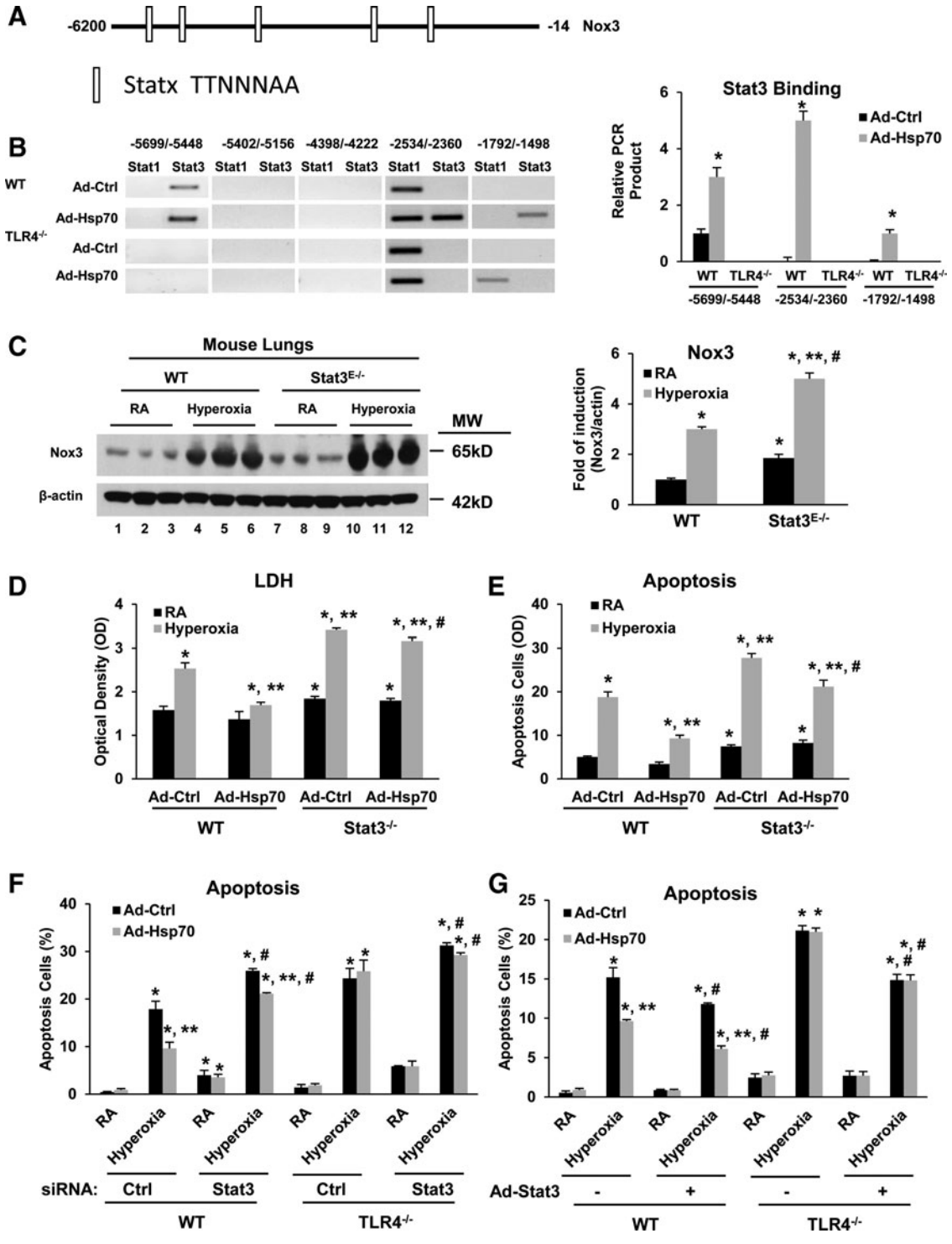

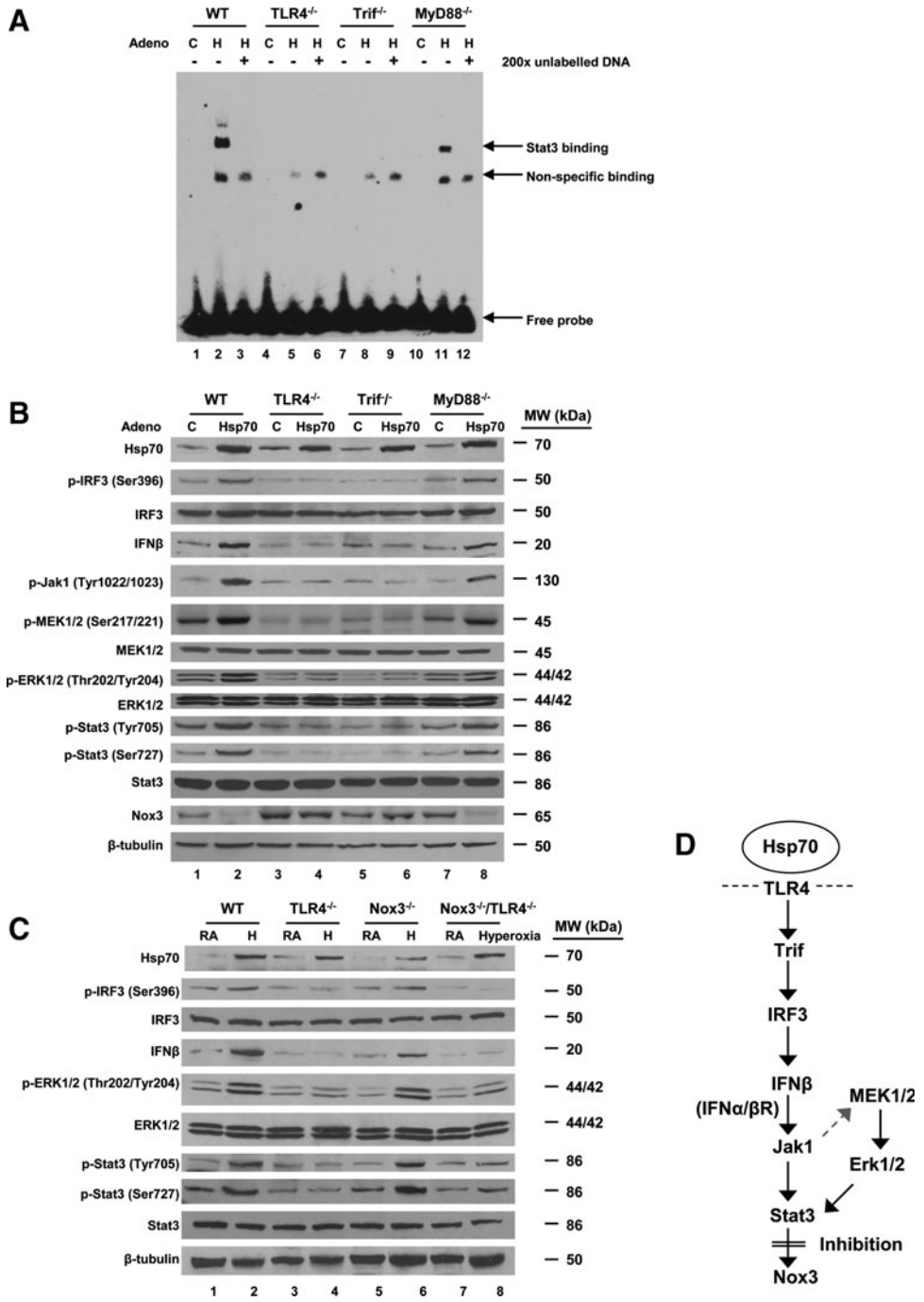

FIG. 8. Stat3 inhibits Nox3 expression *via* a Trif-dependent pathway in MLECs. (A) WT, *TLR4*$^{-/-}$, *Trif*$^{-/-}$, and *MyD88*$^{-/-}$ MLECs were treated with Ad-Ctrl (C) or Ad-Hsp70 (H). Nuclear extracts were mixed with biotin-labeled oligonucleotide-containing Stat3 motif. Competitive inhibition of Stat3 binding was performed with nonlabeled probe (original magnification ×200). Bound complexes were analyzed by electrophoresis. The results are representative of at least three independent experiments. **(B)** WT, *TLR4*$^{-/-}$, *Trif*$^{-/-}$, and *MyD88*$^{-/-}$ MLECs were treated with Ad-Ctrl or Ad-Hsp70. Cell lysates were immunoblotted against antibodies shown on the *left*. β-Tubulin was used as protein loading control. One representative Western blot of three independent experiments is shown. Quantification based on densitometry for the listed proteins relative to β-tubulin is shown in Supplementary Figure S3A. **(C)** WT, *Nox3*$^{-/-}$, *TLR4*$^{-/-}$, and *Nox3*$^{-/-}$/*TLR4*$^{-/-}$ mice were exposed to 72 h of hyperoxia. Lung lysates were immunoblotted against antibodies shown on the *left*. β-Tubulin was used as protein loading control. One representative Western blot of three independent experiments is shown. Quantification based on densitometry for the listed proteins relative to β-tubulin is shown in Supplementary Figure S3B. **(D)** Summary of Hsp70-TLR4-Stat3 signaling. Extracellular Hsp70 interacts with TLR4, which signals through the Trif–IRF3-IFNβ pathway to activate Jak1 and MEK-Erk-Stat3 with subsequent inhibition of Nox3. IFNβ, interferon beta; IRF3, interferon regulatory factor 3.

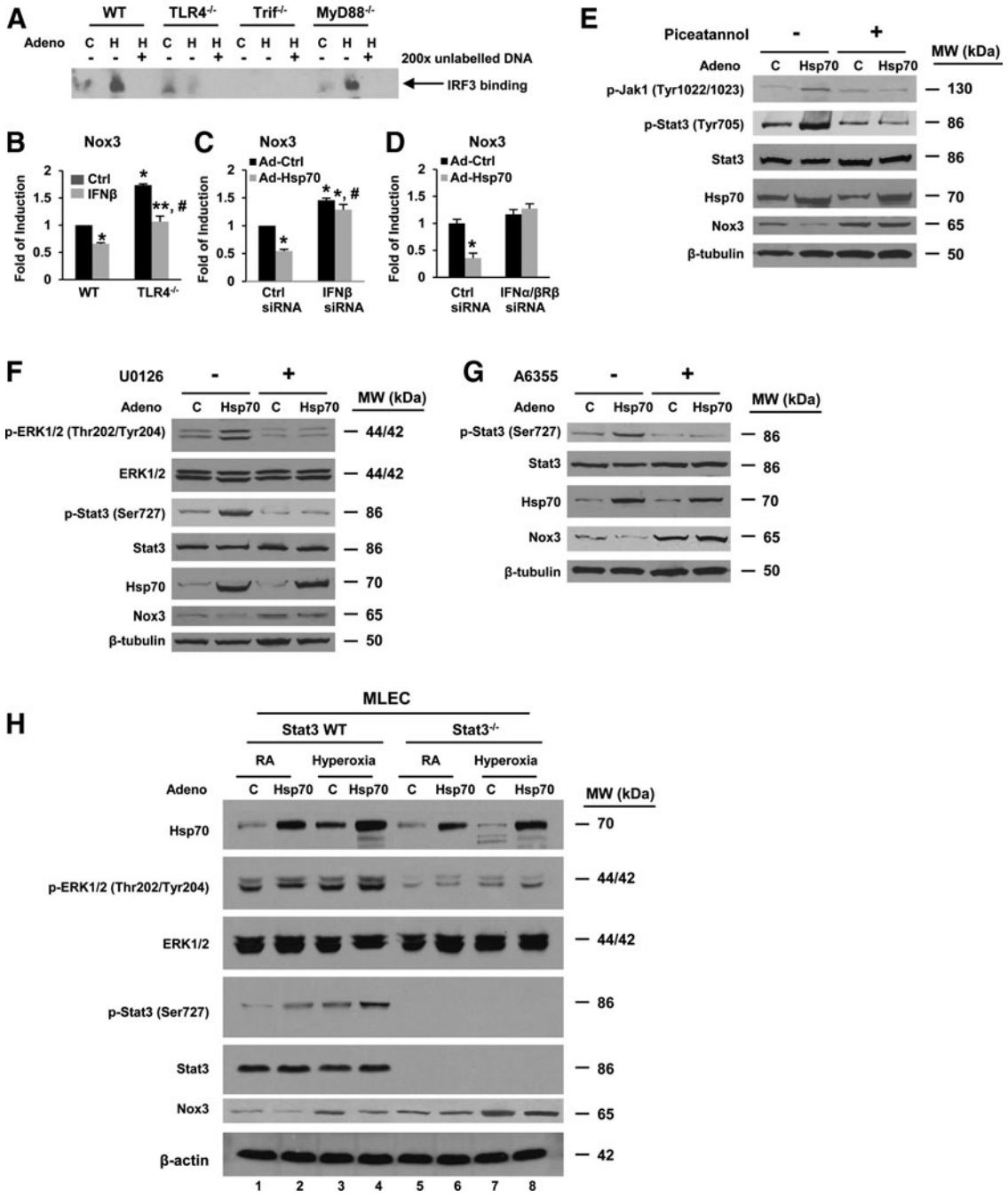

FIG. 9. Signaling mechanisms involved in TLR4-Hsp70-Stat3 inhibition of Nox3. **(A)** WT, *TLR4*$^{-/-}$, *Trif*$^{-/-}$, and *MyD88*$^{-/-}$ MLECs were treated with Ad-Ctrl (C) or Ad-Hsp70 (H). Nuclear extracts were mixed with biotin-labeled oligonucleotide-containing IRF3 binding site on IFNβ promoter. Competitive inhibition of IRF3 binding was performed with nonlabeled probe (original magnification ×200). Bound complexes were analyzed by electrophoresis. The results are representative of at least three independent experiments. **(B)** Nox3 mRNA expression in WT and *TLR4*$^{-/-}$ MLECs was measured by real-time RT-PCR after treatment with or without IFNβ (10^3 unit/ml). The values are expressed as mean ± SD and analyzed by Mann–Whitney test ($n = 6$ for each group). *$p < 0.05$ *versus* WT Ctrl; **$p < 0.05$ *versus* WT IFNβ; $^{\#}p < 0.05$ *versus* *TLR4*$^{-/-}$ Ctrl. Nox3 mRNA expression in WT MLECs transfected with Ctrl siRNA and IFNβ siRNA **(C)** or Ctrl siRNA and IFNα/βRβ siRNA **(D)**, followed by treatment with Ad-Ctrl or Ad-Hsp70, was measured by real-time RT-PCR. The values are expressed as mean ± SD and analyzed by Mann–Whitney test ($n = 6$ for each group). *$p < 0.05$ *versus* Ctrl siRNA; $^{\#}p < 0.05$ *versus* corresponding siRNA. Cell lysates were immunoblotted against antibodies **(E–G)** in WT MLECs pretreated with or without kinase inhibitor for 24 h, followed by treatment with Ad-Ctrl or Ad-Hsp70. JAK1 inhibitor, piceatannol (50 μM) **(E)**, MEK1/2 inhibitor, U0126 (10 μM) **(F)**, or Erk inhibitor, A6355 (50 μM) **(G)**. The results are representative of at least three independent experiments. **(H)** WT and *Stat3*$^{-/-}$ MLECs were treated with Ad-Ctrl or Ad-Hsp70, followed by exposure for 72 h of hyperoxia. Cell lysates were immunoblotted against antibodies shown on the *left*. β-Actin was used as protein loading control. WT and *Stat3*$^{-/-}$ MLECs were treated with Ad-Ctrl or Ad-Hsp70 and were exposed to 72 h of hyperoxia. One representative Western blot of three independent experiments is shown. Quantification based on densitometry for the listed proteins relative to β-tubulin or β-actin is shown in Supplementary Figure S4A–D. IFNα/βRβ, interferon alpha/beta receptor beta.

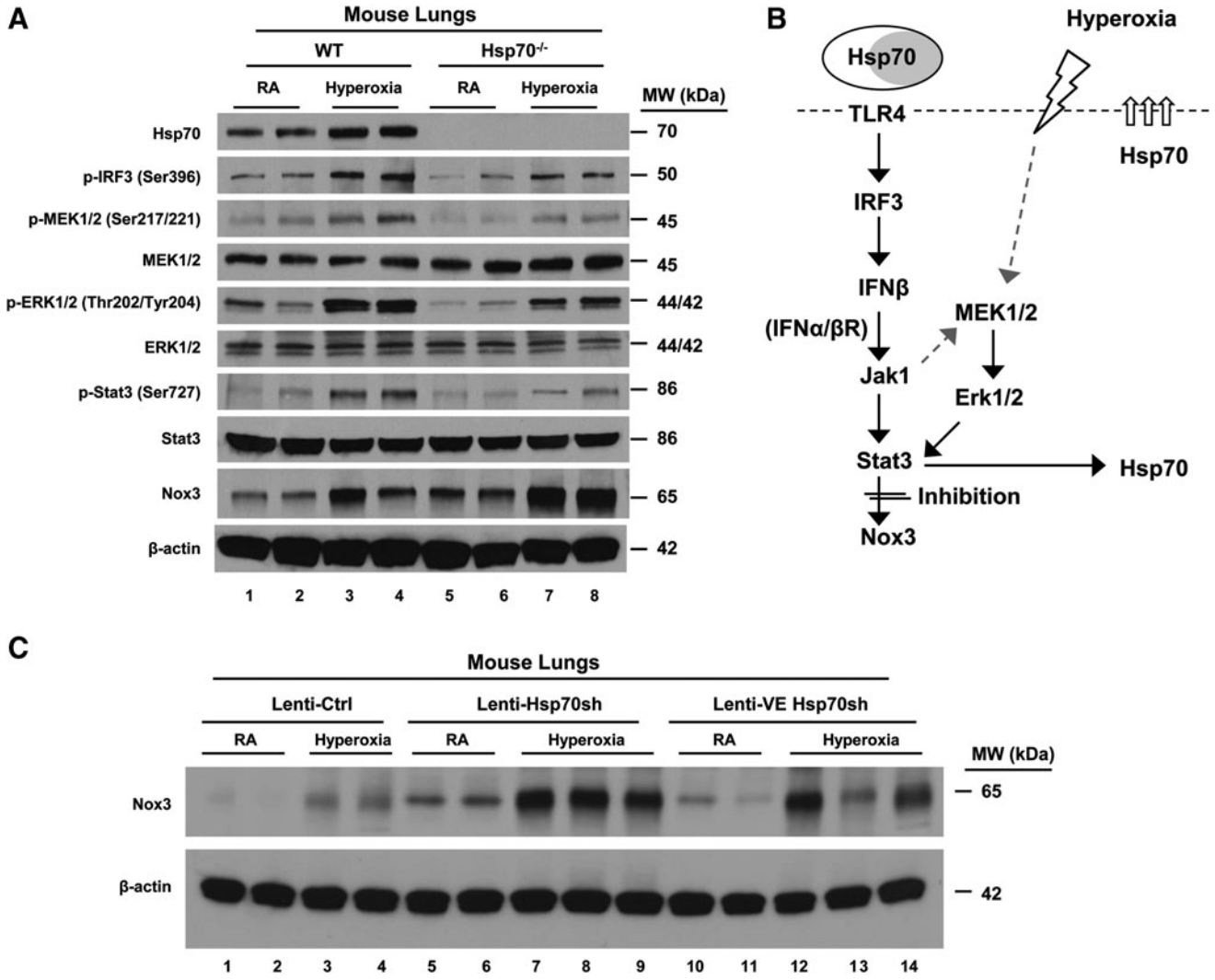

FIG. 10. ***In vivo*** **endothelial targeting of TLR4-Hsp70-Stat3 increases Nox3. (A)** Mice were exposed to RA or 72 h of hyperoxia. Lysates from mouse lungs were isolated and immunoblotted against antibodies as listed. β-Actin was used as protein loading control. **(B)** Summary of Hsp70-TLR4-Stat3 signaling during hyperoxia. Hyperoxia induces Hsp70 secretion from MLECs (*white circle* labeled Hsp70) or other cell types (*gray circle* labeled Hsp70). Extracellular Hsp70 interacts with TLR4 and transduces signal through the Trif-Stat3 pathway to suppress Nox3 expression. **(C)** WT mice were administered intranasal lentivirus (lenti-Ctrl, lenti-Hsp70 miRNA, or lenti-VE Hsp70 miRNA) and exposed to RA or 72 h of hyperoxia. Lysates from mouse lungs were isolated and immunoblotted against antibodies as listed. β-Actin was used as protein loading control. One representative Western blot of three independent experiments is shown. Quantification based on densitometry for the listed proteins relative to β-actin is shown in Supplementary Figure S4E, F. shRNA, short hairpin RNA.

the Institutional Animal Care and Use Committee at Yale University (IACUC).

Measurement of lung injury markers

BAL and protein quantification have been described previously (36). In brief, mice were removed from the exposure chamber and killed after 72 h of hyperoxia exposure. BAL was performed twice with 0.8 ml phosphate-buffered saline (PBS; pH 7.4). Cell pellets were pooled, resuspended in PBS, and counted. BAL cells were cytocentrifuged onto microscope slides at 800 rpm for 5 min using 100 μl cell suspension containing 5×10^5 cells/ml in PBS. The cytocentrifuge preparations were quantified in Cytospin preparations (Perbio Science) after staining with Diff-Quik dye (Dade Behring). The supernatant was used for bronchoalveolar lavage fluid protein determination. The protein concentration in each sample was determined by the BCA Protein Assay Reagent (Thermo Fisher Scientific, Inc.), using BSA as the standard.

Isolation of primary MLECs and hyperoxia exposure

Isolation of MLECs from mouse lungs has been described previously (35-38). In brief, microvascular endothelial cells were isolated from lungs of animals 4 weeks old with magnetic beads coated with anti-mouse CD102 antibody (clone 3C4; BD Biosciences) and anti-mouse CD31 antibody (clone MEC 13.3; BD Biosciences) (5 μg/4×10^6 beads, Dynabeads M-450; Dynal). Cultures were grown to confluence and

selected twice before being plated for experiments. MLECs were treated with lentivirus at a concentration of 2×10^6 transduction units (TUs) to 10^5 cells. After 24 h of incubation, the cells were collected and subjected to hyperoxia for 72 h.

LDH assay

LDH was detected by the Cytotoxicity Detection Kit (Roche) in the culture supernatant of MLECs exposed to hyperoxia or kept in room air. LDH was also detected in mouse BAL using the same procedure.

Amplex Red assay

Amplex® Red Hydrogen Peroxide/Peroxidase Assay Kit (Thermo Fisher Scientific, Inc.) was used to check H_2O_2 released from mouse lung in BAL according to the manufacturer's protocol.

TBARS assay

Malondialdehyde (MDA) levels were evaluated in the homogenized lung tissue using a TBARS Assay Kit (Cayman Chemical). Protein was extracted from lungs, and 10 μg was processed for TBARS assay according to the manufacturer's protocol. The colorimetric measurement was quantified at 540 nm in a kinetic microplate reader (Vmax; Molecular Devices).

Total antioxidant capacity

Protein was extracted from lungs and 10 μg was processed for the quantitative assay with the Total Antioxidant Potential Kit (Oxis International, Inc.), as described previously (33).

Construction of lentiviral vectors and administration

Lentivirus miRNA vectors with VE-Cad promoter have been described previously (36). Hsp70 knockdown vectors were designed by using target site 600–620 (GenBank accession NM_010479.2), 5′-ATCTCCTTCATCTTCGTC AGC-3′. We used Thermo Fisher Scientific, Inc., Scientific–Invitrogen's online RNAi Designer tool to design premiRNA stem-loop/siRNA hybrid sequences according to instructions. Two oligos, 5′-TGCTGATCTCCTTCATCTTCGTCA GCGTTTTGGCCACTGACTGACGCTGACGAATGAAG GAGAT-3′ and 5′-CCTGATCTCCTTCATTCGTCAGCG TCAGTCAGTGGCCAAAACGCTGACGAAGATGAAGG AGATC-3′, were annealed and ligated into pcDNA6.2-GW/ EGFP-miR (Thermo Fisher Scientific, Inc.) according to the manufacturer's instructions.

The constructs were confirmed by sequencing. The pcDNA6.2-GW/EGFP-miR-neg control plasmid was provided by Thermo Fisher Scientific, Inc. The lentiviral constructs of EGFP-Hsp70-RNAi were constructed by first amplifying the fragments from pcDNA6.2-GW/EGFP-miR with primers, sense: 5′-AGGCGCGCCTGGCTA ACTA-GAGAAC-3′ and antisense: 5′-GGAATTCTATCTC GAGTGCGGC-3′, and by digestion of the PCR product with *Asc*I and *Eco*RI enzymes. This fragment then was inserted into the *Asc*I and *Eco*RI sites of FVEW or FUW (36) to generate lenti-VE Hsp70sh or lenti-Hsp70sh vectors. TLR4-knockdown vectors (lenti-TLR4sh and lenti-VE TLR4sh) were constructed with similar strategy and were designed using target site 550–570 (GenBank accession NM_021297.2), 5′-GTACATGTGGATCTTTCTTAT-3′ (28).

Lentiviral TLR4 overexpression (lenti-VE hTLR4) has been described previously (28). It was constructed by amplifying the fragments from CD4hTLR4 construct (22) with primers: sense: 5′-AGGCGCGCCACCACCATGTGCCGA GCCAT-3′ and antisense: 5′-GGAATTCTCAGATAGATG TTGCTTCCT-3′. The CD4hTLR4 was recovered from the PCR fragment by *Asc*I and *Eco*RI digestion and then inserted into the *Asc*I and *Eco*RI sites of FVEW to generate lenti-VE hTLR4 or of FUW to generate lenti-hTLR4. Lenti-mNox3 was constructed by amplifying the fragments from pcDNA3.1-mNox3 (Addgene plasmid No. 58337) with primers: sense: 5′-GTTAACATGCCGGTGTGCTGGATTCT-3′ and antisense: 5′-GGCGCGCCCTAGAAGTTTTCCTTGTT-3′. The mNox3 was recovered from the PCR fragment by *Hpa*I and *Asc*I digestion and then inserted into the *Hpa*I and *Asc*I sites of FUW to generate lenti-mNox3.

All restriction endonucleases were purchased from New England Biolabs. Lentivirus production, titer measurement, and intranasal administration were previously described (36). In lentivirus delivery experiments, 1×10^8 TUs of the package lentiviral particles were administered intranasally to 6- to 8-week-old mice through a published intranasal method (36).

Nox3 expression in endothelium modified with endothelial-targeting lentivirus

Endothelial cells ($CD31^+$, $CD45^-$) were isolated using Miltenyi Biotec magnetic columns or Dynabead Tosyl-activated Dynabeads and the autoMACS system using manufacturer-supplied antibodies, according to the manufacturers' instructions. Lungs were harvested from mice, minced into small pieces in PBS on ice, and filtered through 70-μm nylon meshes to created single-cell suspensions. Cell labeling with magnetic antibodies and cell separation were performed according to the manufacturer's instructions. Total lung cell suspensions were first depleted of $CD45^+$ cells and then positively selected for $CD31^+$ cells. Each cell subfraction was dissolved in TRIzol buffer and RNA was isolated. For real-time PCR, the Nox3 primers were used. GAPDH was amplified as a control and performed for each group of cells, such as $CD45^-/CD31^+$, $CD45^-/CD31^-$, BAL macrophages, and total lung lyses.

Histology

For each experimental condition, 6–10 mice were analyzed. Mice were anesthetized, the pulmonary intravascular space was cleared, and whole lungs were dissected from mice and immediately fixed in buffered formalin at 4°C overnight and processed for paraffin embedding. Histological analysis was performed on 5-μm sections by the Yale Histopathology Services. Lung sections were processed for TUNEL, immunohistochemistry, and immunofluorescence microscopy as described below.

TUNEL assay

We used the *in situ* cell death detection kit according to the manufacturer's protocol (Roche Molecular Biochemicals). Sections of formalin-fixed, paraffin-embedded lung tissue were deparaffinized and rehydrated, rinsed with PBS, and digested with proteinase K (Roche Molecular Biochemicals)

at a concentration of 20 mg/ml for 20 min. After PBS washes, sections were incubated with TUNEL reaction mixture at 37°C for 1 h, then incubated with antifluorescein-conjugated horseradish peroxidase at 37°C for 30 min. Sections were washed twice with PBS and stained with nitro blue tetrazolium/5-bromo-4-chloro-3-indolyl phosphate substrate solution before counterstaining with nuclear fast red. Apoptotic and normal cells were observed under a light microscope. Normal cells exhibited red nuclear staining, whereas TUNEL-positive cells, indicating cell death/apoptosis, exhibited purple nuclear staining. Five hundred cells were counted for each sample and the number of apoptotic cells is expressed as a percentage of the total counted.

Immunohistochemistry and immunofluorescence microscopy

Briefly, formalin-fixed, paraffin-embedded lung tissue sections were deparaffinized with xylene, rehydrated gradually with graded alcohol solutions, and then washed with deionized water. After heat-induced antigen retrieval with target retrieval solution (Dako), pH 6.0, in a microwave pressure cooker, sections were blocked with serum-free protein block buffer (Dako) for 1 h. Sections were incubated with a 1:200 dilution of anti-Nox3 (Santa Cruz Biotechnology, Inc.) antibody at 4°C overnight. After PBS washes, sections were incubated with a biotinylated rabbit anti-goat secondary Ab (Vector Laboratories) for immunohistochemistry or a secondary antibody (Alexa Fluor® 594 goat anti-rabbit IgG from Invitrogen at 1:300 dilution) for immunofluorescence at room temperature for 1 h.

For immunohistochemistry, samples were washed thrice by immersing in PBS for 5 min and incubated with the Vectastain Universal ABC-AP kit according to the instructions. The samples were developed with the Vector Red alkaline phosphatase substrate kit.

For immunofluorescence, samples were washed thrice by immersing in PBS for 5 min and then mounted with Prolong Gold mounting media with DAPI (Thermo Fisher Scientific, Inc.). Labeled cells were observed under dark field in independent fluorescence channels using an automated Olympus BX-61 microscope (320 and 340 objective lens; NA 0.50; Olympus Imaging America, Inc.) equipped with a cooled CCD camera (Q-Color 5; Olympus) and QCapture Pro 6.0 software (QImaging). Exposure time was set as 100 mS for DAPI and 300 mS for the positive signal. Images were analyzed and quantified using ImageJ software (http://imagej.nih.gov/ij/). Data are representative of at least 20 images.

Western blot analyses

Lung or MLEC protein analyses were performed as previously described with minor modifications (36). Whole lung tissues were homogenized in 62.5 m*M* Tris buffer, and cell pellets were lysed in 1× RIPA lysis buffer (Thermo Fisher Scientific, Inc.). The protein concentrations of the lysates were determined by BCA Protein Assay (Thermo Fisher Scientific, Inc.). Samples were electrophoresed in a 12% ready-made Tris-HCl gel (Bio-Rad Laboratories) and electrophoretically transferred onto a nitrocellulose membrane. The membranes were then incubated overnight with anti-Hsp70 (Stressgen), pSer-IRF3, IRF3, pTyr-Jak1, pSer-MEK1/2, MEK1/2, pERK1/2, ERK1/2, pTyr-Stat3, pSer-Stat3, Stat3 (Cell Signaling Technology), Nox3, IFNβ, β-tubulin, and β-actin (Santa Cruz Biotechnology, Inc.) antibodies with 1:1000 dilution in 5% BSA. The membranes were incubated with HRP-conjugated secondary IgG Ab, followed by the detection of signal with a chemiluminescence LumiGLO detection kit (Cell Signaling Technology).

Apoptosis assays

The fluorescence-activated cell sorter (FACS) was used to detect Annexin V-fluorescein isothiocyanate labeling (BD Biosciences) on MLECs as described previously (32). Briefly, MLECs were washed with cold PBS and resuspended with binding buffer (BD Biosciences); a solution containing 1×10^5 cells was transferred to a 5-ml tube, and 5 μl each of Annexin V and propidium iodide was added. Binding buffer was then added to each tube and analyzed by FACS (BD Biosciences). Data were analyzed with FlowJo software.

Flow cytometry assays for ROS

CM-H2DCFDA and MitoSOX Red (Invitrogen) were used to determine levels of ROS in endothelial cells. Cells were seeded onto culture plates 1 day before the experiment. Cells were washed and exposed to CM-H2DCFDA (5 μM) or MitoSOX Red (2.5 m*M*) in regular media and kept at 37°C for 25 min. The cells were washed with PBS and then detached gently with 0.4 *M* EDTA and analyzed on a BD FACSCaliber machine. CM-H2DCFDA was detected in the FL-1 channel, and MitoSOX Red was detected in the FL-3 channel.

DHE staining and fluorescence microscopy

MLECs were adjusted to a density of 1×10^5 cells/ml and seeded on poly-L-lysine-coated coverslips (BD Biosciences) in a volume of 200 μl (2×10^4 cells). After specific exposure as mentioned, live cells were incubated in the presence of 2 μM DHE (Thermo Fisher Scientific, Inc.) and in the absence or presence of SOD (600 U/ml) or DPI (10 μM) (Sigma-Aldrich Corp) for 30 min at 37°C. Samples were washed thrice by immersing in PBS for 5 min and then fixed with 4% paraformaldehyde for 15 min, washed once in PBS, and then mounted with Prolong Gold mounting media with DAPI (Thermo Fisher Scientific, Inc.). Labeled cells were observed under dark field in independent fluorescence channels using an automated Olympus BX-61 microscope (320 and 340 objective lens; NA 0.50; Olympus Imaging America, Inc.) equipped with a cooled CCD camera (Q-Color 5; Olympus) and QCapture Pro 6.0 software (QImaging).

Exposure time was set as 100 mS for DAPI and 300 mS for DHE signal. Images were analyzed and quantified using ImageJ software (http://imagej.nih.gov/ij/). The DHE and DAPI fluorescence intensity of each image was measured, relative DHE was analyzed as described (30). Data are representative of at least 20 images.

Measurement of oxidative stress and superoxide level

The oxidative stress and superoxide levels were measured by a commercial kit according to the manufacturer's instructions (Total ROS/Superoxide Detection Kit; Enzo Life Sciences). After specific exposure as mentioned, live cells were incubated with 1 μM ROS/Superoxide Detection mix

for 60 min at 37°C. The ROS inducer, pyocyanin (Pyo, 200 μM), or the ROS inhibitor, N-acetyl-L-cysteine (NAC, 5 mM), was incubated with WT MLECs as the positive or negative control. Changes in fluorescence intensity were measured using a fluorometer (SpectraMAX Gemini XS; Molecular Devices) at excitation/emission wavelengths of 488/520 nm (oxidative stress) and 550/610 nm (superoxide). For flow cytometry, collect cells after specific exposure as mentioned, wash cells once with wash buffer, resuspend cell pellet in 500 μl of ROS/Superoxide Detection solution, stain cells for 30 min at 37°C in the dark, and simultaneously treat the cells with control agent (Pyo or NAC).

The cells were analyzed on the BD FACSCaliber machine. Cells with increased production of superoxide demonstrate bright orange fluorescence and will be detected using the FL2 channel. Such cells will appear in the two upper quadrants of a log FL1 (x-axis) *versus* a log FL2 (y-axis) dot plot. Cells with increased levels of oxidative stress demonstrate a bright green staining in the presence of the oxidative stress detection reagent and can be registered in the FL1 channel. Such cells will appear in the upper and lower right quadrants of a log FL1 (x-axis) *versus* a log FL2 (y-axis) dot plot.

Enzyme-linked immunosorbent assay

Mice were exposed to 72 h of hyperoxia or kept at room air. BAL was collected, serially diluted, and measured for TNFα, IL-1β, and IL-6 by enzyme-linked immunosorbent assay (BD Biosciences) as per the manufacturer's instructions.

Total antioxidant capacity

Protein was extracted from total lungs and 10 μg was processed for the quantitative assay with Total Antioxidant Potential kit (Oxis International, Inc.), as described (33). Briefly, lung tissue proteins were incubated with Bathocuproine (2,9-dimethyl-4,7-diphenyl-1,10-phenanthroline) and Cu^{2+}-containing reagents. Bathocuproine selectively forms a 2:1 complex with Cu^{+}, which has a maximum absorbance at 490 nm. A standard of a known uric acid concentration was used to create a calibration curve. Results are expressed as mM copper-reducing equivalents per μg protein.

Protein kinase inhibitors

JAK1 inhibitor, piceatannol, MEK1/2 inhibitor, U0126, and Erk inhibitor, A6355, were purchased from Sigma-Aldrich.

Preparation of siRNA and transfection of siRNA duplexes

Mouse Nox3 siRNA (sc-45485), IFNβ siRNA (sc-39604), and IFNα/βRβ (sc-40092) siRNA were purchased from Santa Cruz Biotechnology, Inc. Stat3 siRNA was described previously (34). The sense and antisense strands of mouse Stat3 siRNA were sense: 5′-ACAUGGAGGAGUCUAACAA-3′, antisense: 5′-UUGUUAGACUCCUCCAUGU-3′; nonspecific siRNA scrambled duplex probes (sense: 5′-GCGCGC UUUGUAGGAUUCG-3′; antisense: 5′-CGAAUCCUACA AAGCGCGC-3′) were synthesized by Dharmacon Research as previously described (33). MLECs were seeded into a 6- or 12-well plate 1 day before transfection using 40% Dulbecco's modified Eagle medium and 40% F12 TCM supplemented with 20% fetal bovine serum, without antibiotics. At the time of transfection with siRNA, the cells were 50%–60% confluent. Lipofectamine 2000 Reagent (Invitrogen) was used as the transfection agent, according to the manufacturer's manual, for 48 h. The experiments were performed after fresh medium change (38).

Overexpression of Stat3 and Hsp70 in MLECs

A replication-deficient adenoviral vector encoding Stat3-C (constitutively active form of Stat3, AxCAS3-C) has been described (34). Ad-Hsp70 has been described (38). Ad-null, an adenovirus empty vector, was used as a control (Vector BioLabs). For cell experiments, adenovirus was transfected at 2.5 multiplicity of infection (the average number of phage particles that infect a single cell) 24 h before hyperoxia exposure (38).

Total RNA isolation and real-time RT-PCR amplification

Total RNA was extracted from lungs or cells by using TRIzol reagent according to the manufacturer's protocol (Gibco BRL). DNase digestion was performed during RNA isolation. First-strand complementary DNA (cDNA) was synthesized by using Superscript II Reverse Transcriptase (Invitrogen) with random hexamers; conditions were 10 min at 25°C, 30 min at 48°C, and 5 min at 95°C. Real-time RT-PCR reactions were carried out in Power SsoFast EvaGreen Supermix (Bio-Rad Laboratories) and an ABI Prism 7000 Sequence Detection System (Applied Biosystems).

For real-time PCR, the Nox3 primers were sense 5′-GCTGGCTGC ACTTTCCAAA-3′ and antisense 5′-AAGGTGCGGACTG GATTGAG-3′. TLR4 primers were sense 5′-CAGCAAAG TCCCTGATGACA and antisense 5′-AGAGGTGGTGTA AGCCATGC-3′. IL-6 primers were sense 5′-TAGTCCTTC CTACCCCAATTTCC-3′ and antisense 5′-TTGGTCCTTA GCCACTCCTTC-3′. GAPDH primers were sense 5′-TGTG TCCGTCGTGGATCTGA-3′ and antisense 5′-CCTGCTT CACCACCTTCTTGAT-3′. The primers were designed as intron spanning.

Real-time PCR conditions were 95°C for 10 min and 40 cycles at 95°C for 15 s, followed by 60°C for 1 min. The relative values of gene expression were calculated from the accurate threshold cycle (CT), which is the PCR cycle at which an increase in reporter fluorescence from dye can first be detected above a baseline signal. The CT values for GAPDH were subtracted from the CT values for Nox3 in each well to calculate ΔCT. The ΔCT values for each sample were averaged. To calculate the fold induction over controls ($\Delta\Delta$CT), the average ΔCT values calculated for WT tissue/cells were subtracted from ΔCT values calculated for knockout tissue/cells. Next, the fold induction for each well was calculated by the $2^{-\Delta\Delta CT}$ formula. The fold induction values for replicate wells were averaged, and data are presented as mean ± standard deviation (SD) of triplicate wells.

Electrophoretic mobility shift assays

EMSAs of nuclear protein isolated from MLECs were performed as previously described with minor modifications (38). Nuclear extracts were prepared using an NE-PER Nuclear and Cytoplasmic Extraction Reagent Kit (Thermo Fisher Scientific, Inc.), according to the manufacturer's

protocol. The Stat3 site was synthesized as complementary oligodeoxyribonucleotide strands. The sequence of Stat3 consensus oligonucleotides was 5′-GATCCTTCTGGGA ATTCCTAGATC-3′ (Santa Cruz Biotechnology, Inc.). The sequence of IRF3 binding site on IFNβ promoter was 5′-GAGGAAAACTGAAAGGGAGAACTGAAAGTGGGA-3′.

The DNA-binding ability in the nuclear extracts was assessed by EMSA with biotin-labeled double-stranded probes. EMSA was carried out using the LightShift Chemiluminescent EMSA Kit (Pierce). Specific binding was confirmed using 200-fold excess of unlabeled probe as a specific competitor. Protein-DNA complexes were separated using a 6% non-denaturing acrylamide gel electrophoresis and then transferred to positively charged nylon membranes and cross-linked by UV irradiation. Gel shifts were visualized with streptavidin HRP, according to standard protocols.

ChIP assays

ChIP assays were performed using the ChIP kit (EMD Millipore), according to the manufacturer's instructions. Briefly, immunoprecipitations will be performed using 3 μg antibody against protein of interest (*e.g.*, Stat3 or Stat1). Negative controls with normal IgG and no antibody will also be used. Primers used to amplify the Nox3 promoter sequences are (forward and reverse, respectively): 5′-TTC AAACAGGGCCACTTAG-3′and 5′-TTCCACTTGGGAC AAACAT-3′ for −5699/−5448; 5′-CTCAAGAAAGCCAG ACCA-3′ and 5′-TGTCCATCACAATATCCC-3′ for −5402/−5156; 5′-TATGCCAACAATACTTTACG-3′and 5′-GCAG TGAGTGCCACCTT-3′ for −4398/−4222; 5′-TGTT TAC-TACCACATCCACG-3′ and 5′-CCACCTAGCCCGA CCT AT-3′ for −2534/−2360; and 5′-GTGAGCCTCAATA TGCC −3′ and 5′-TCTGAGCTTAGCGTTT-3′ for −1792/−1498. PCR conditions are as follows: 95°C for 5 min, then 33 cycles at 95°C for 30 s, 55°C for 30 s, and 72°C for 30 s, followed by 72°C for 7 min. Aliquots of chromatin will also be analyzed before immunoprecipitation and serve as an input control.

Laser capture microdissection and RNA extraction

Laser capture microdissection (LCM) was used to selectively dissect sections of large airway, alveolar tissue, and blood vessels from lung histological sections for quantitation of mRNA by real-time RT-PCR, as described previously (26). To prepare mouse lungs for microdissection, the trachea was cannulated and the lungs were dissected from the chest cavity. The lungs were inflated with 50% Tissue-Tek OCT in PBS, the trachea was clamped, and the inflated lungs were embedded in optimum cutting temperature (OCT) (Sakura Finetek). Sections (10 μm) were cut with a refrigerated microtome, fixed in cold 70% ethanol, and stained with hematoxylin and eosin. For LCM, we used the Leica AS LMD apparatus (Leica) and microdissected sections from large airway, blood vessels, and alveolar tissue. The RNeasy Micro Kit (Qiagen) was used for RNA isolation from the OCT-embedded microdissected specimens.

Statistics

Data are expressed as mean ± SD and analyzed by the Mann–Whitney test or Student's *t* test. Significant difference was accepted at $p < 0.05$. Survival curves were produced with Prism software (GraphPad). Statistical comparisons for survival curves were performed with the log rank (Mantel-Cox) test.

Acknowledgments

The authors thank Dr. Tej Pandita for the *Hsp70*$^{-/-}$ mice, Dr. S. Akira for *TLR4*$^{-/-}$ mice, and Dr. X. Fu for endothelial Stat3-deficient mice (*Stat3*$^{E-/-}$). P.J.L. was supported by NIH Grants, HL 071595, HL 090660, and FAMRI 82384.

Author Disclosure Statement

No competing financial interests exist.

References

1. Banfi B, Malgrange B, Knisz J, Steger K, Dubois-Dauphin M, and Krause KH. NOX3, a superoxide-generating NADPH oxidase of the inner ear. *J Biol Chem* 279: 46065–46072, 2004.
2. Benipal B, Feinstein SI, Chatterjee S, Dodia C, and Fisher AB. Inhibition of the phospholipase A2 activity of peroxiredoxin 6 prevents lung damage with exposure to hyperoxia. *Redox Biol* 4: 321–327, 2015.
3. Cai H, Dikalov S, Griendling KK, and Harrison DG. Detection of reactive oxygen species and nitric oxide in vascular cells and tissues: comparison of sensitivity and specificity. *Methods Mol Med* 139: 293–311, 2007.
4. Cantu E, Shah RJ, Lin W, Daye ZJ, Diamond JM, Suzuki Y, Ellis JH, Borders CF, Andah GA, Beduhn B, Meyer NJ, Ruschefski M, Aplenc R, Feng R, and Christie JD; Lung Transplant Outcomes Group I. Oxidant stress regulatory genetic variation in recipients and donors contributes to risk of primary graft dysfunction after lung transplantation. *J Thorac Cardiovasc Surg* 149: 596–602, 2015.
5. Cheng G, Cao Z, Xu X, van Meir EG, and Lambeth JD. Homologs of gp91phox: cloning and tissue expression of Nox3, Nox4, and Nox5. *Gene* 269: 131–140, 2001.
6. Dikalov SI and Harrison DG. Methods for detection of mitochondrial and cellular reactive oxygen species. *Antioxid Redox Signal* 20: 372–382, 2014.
7. Frame FM, Hager S, Pellacani D, Stower MJ, Walker HF, Burns JE, Collins AT, and Maitland NJ. Development and limitations of lentivirus vectors as tools for tracking differentiation in prostate epithelial cells. *Exp Cell Res* 316: 3161–3171, 2010.
8. Gao D, Nong S, Huang X, Lu Y, Zhao H, Lin Y, Man Y, Wang S, Yang J, and Li J. The effects of palmitate on hepatic insulin resistance are mediated by NADPH Oxidase 3-derived reactive oxygen species through JNK and p38MAPK pathways. *J Biol Chem* 285: 29965–29973, 2010.
9. Geiszt M and Leto TL. The Nox family of NAD(P)H oxidases: host defense and beyond. *J Biol Chem* 279: 51715–51718, 2004.
10. Hecker L, Logsdon NJ, Kurundkar D, Kurundkar A, Bernard K, Hock T, Meldrum E, Sanders YY, and Thannickal VJ. Reversal of persistent fibrosis in aging by targeting Nox4-Nrf2 redox imbalance. *Sci Transl Med* 6: 231ra47, 2014.
11. Hunt CR, Dix DJ, Sharma GG, Pandita RK, Gupta A, Funk M, and Pandita TK. Genomic instability and enhanced radiosensitivity in Hsp70.1- and Hsp70.3-deficient mice. *Mol Cell Biol* 24: 899–911, 2004.

12. Kano A, Wolfgang MJ, Gao Q, Jacoby J, Chai GX, Hansen W, Iwamoto Y, Pober JS, Flavell RA, and Fu XY. Endothelial cells require STAT3 for protection against endotoxin-induced inflammation. *J Exp Med* 198: 1517–1525, 2003.
13. Konior A, Schramm A, Czesnikiewicz-Guzik M, and Guzik TJ. NADPH oxidases in vascular pathology. *Antioxid Redox Signal* 20: 2794–2814, 2014.
14. Lambeth JD. NOX enzymes and the biology of reactive oxygen. *Nat Rev Immunol* 4: 181–189, 2004.
15. Lambeth JD, Kawahara T, and Diebold B. Regulation of Nox and Duox enzymatic activity and expression. *Free Radic Biol Med* 43: 319–331, 2007.
16. Liu X, Pei C, Yan S, Liu G, Liu G, Chen W, Cui Y, and Liu Y. NADPH oxidase 1-dependent ROS is crucial for TLR4 signaling to promote tumor metastasis of non-small cell lung cancer. *Tumour Biol* 36: 1493–1502, 2015.
17. Montezano AC, Dulak-Lis M, Tsiropoulou S, Harvey A, Briones AM, and Touyz RM. Oxidative stress and human hypertension: vascular mechanisms, biomarkers, and novel therapies. *Can J Cardiol* 31: 631–641, 2015.
18. Morimoto H, Kanatsu-Shinohara M, and Shinohara T. ROS-generating oxidase Nox3 regulates the self-renewal of mouse spermatogonial stem cells. *Biol Reprod* 92: 147, 2015.
19. Paffenholz R, Bergstrom RA, Pasutto F, Wabnitz P, Munroe RJ, Jagla W, Heinzmann U, Marquardt A, Bareiss A, Laufs J, Russ A, Stumm G, Schimenti JC, and Bergstrom DE. Vestibular defects in head-tilt mice result from mutations in Nox3, encoding an NADPH oxidase. *Genes Dev* 18: 486–491, 2004.
20. Park HS, Jung HY, Park EY, Kim J, Lee WJ, and Bae YS. Cutting edge: direct interaction of TLR4 with NAD(P)H oxidase 4 isozyme is essential for lipopolysaccharide-induced production of reactive oxygen species and activation of NF-kappa B. *J Immunol* 173: 3589–3593, 2004.
21. Peshavariya HM, Dusting GJ, and Selemidis S. Analysis of dihydroethidium fluorescence for the detection of intracellular and extracellular superoxide produced by NADPH oxidase. *Free Radic Res* 41: 699–712, 2007.
22. Qureshi ST, Zhang X, Aberg E, Bousette N, Giaid A, Shan P, Medzhitov RM, and Lee PJ. Inducible activation of TLR4 confers resistance to hyperoxia-induced pulmonary apoptosis. *J Immunol* 176: 4950–4958, 2006.
23. Ruwanpura SM, McLeod L, Lilja AR, Brooks G, Dousha LF, Seow HJ, Bozinovski S, Vlahos R, Hertzog PJ, Anderson GP, and Jenkins BJ. Non-essential role for TLR2 and its signaling adaptor Mal/TIRAP in preserving normal lung architecture in mice. *PLoS One* 8: e78095, 2013.
24. Rybak LP, Mukherjea D, Jajoo S, Kaur T, and Ramkumar V. siRNA-mediated knock-down of NOX3: therapy for hearing loss? *Cell Mol Life Sci* 69: 2429–2434, 2012.
25. Sanders YY, Liu H, Liu G, and Thannickal VJ. Epigenetic mechanisms regulate NADPH oxidase-4 expression in cellular senescence. *Free Radic Biol Med* 79: 197–205, 2015.
26. Siner JM, Jiang G, Cohen ZI, Shan P, Zhang X, Lee CG, Elias JA, and Lee PJ. VEGF-induced heme oxygenase-1 confers cytoprotection from lethal hyperoxia in vivo. *FASEB J* 21: 1422–1432, 2007.
27. Stowe DF and Camara AK. Mitochondrial reactive oxygen species production in excitable cells: modulators of mitochondrial and cell function. *Antioxid Redox Signal* 11: 1373–1414, 2009.
28. Takyar S, Zhang Y, Haslip M, Jin L, Shan P, Zhang X, and Lee PJ. An endothelial TLR4-VEGFR2 pathway mediates lung protection against oxidant-induced injury. *FASEB J* 30: 1317–1327, 2016.
29. Valente AJ, El Jamali A, Epperson TK, Gamez MJ, Pearson DW, and Clark RA. NOX1 NADPH oxidase regulation by the NOXA1 SH3 domain. *Free Radic Biol Med* 43: 384–396, 2007.
30. Wojtala A, Bonora M, Malinska D, Pinton P, Duszynski J, and Wieckowski MR. Methods to monitor ROS production by fluorescence microscopy and fluorometry. *Methods Enzymol* 542: 243–262, 2014.
31. Wu F, Szczepaniak WS, Shiva S, Liu H, Wang Y, Wang L, Wang Y, Kelley EE, Chen AF, Gladwin MT, and McVerry BJ. Nox2-dependent glutathionylation of endothelial NOS leads to uncoupled superoxide production and endothelial barrier dysfunction in acute lung injury. *Am J Physiol Lung Cell Mol Physiol* 307: L987–L997, 2014.
32. Zhang X, Shan P, Jiang D, Noble PW, Abraham NG, Kappas A, and Lee PJ. Small interfering RNA targeting heme oxygenase-1 enhances ischemia-reperfusion-induced lung apoptosis. *J Biol Chem* 279: 10677–10684, 2004.
33. Zhang X, Shan P, Jiang G, Cohn L, and Lee PJ. Toll-like receptor 4 deficiency causes pulmonary emphysema. *J Clin Invest* 116: 3050–3059, 2006.
34. Zhang X, Shan P, Jiang G, Zhang SS, Otterbein LE, Fu XY, and Lee PJ. Endothelial STAT3 is essential for the protective effects of HO-1 in oxidant-induced lung injury. *FASEB J* 20: 2156–2158, 2006.
35. Zhang X, Shan P, Qureshi S, Homer R, Medzhitov R, Noble PW, and Lee PJ. Cutting edge: TLR4 deficiency confers susceptibility to lethal oxidant lung injury. *J Immunol* 175: 4834–4838, 2005.
36. Zhang Y, Jiang G, Sauler M, and Lee PJ. Lung endothelial HO-1 targeting in vivo using lentiviral miRNA regulates apoptosis and autophagy during oxidant injury. *FASEB J* 27: 4041–4058, 2013.
37. Zhang Y, Sauler M, Shinn AS, Gong H, Haslip M, Shan P, Mannam P, and Lee PJ. Endothelial PINK1 mediates the protective effects of NLRP3 deficiency during lethal oxidant injury. *J Immunol* 192: 5296–5304, 2014.
38. Zhang Y, Zhang X, Shan P, Hunt CR, Pandita TK, and Lee PJ. A protective Hsp70-TLR4 pathway in lethal oxidant lung injury. *J Immunol* 191: 1393–1403, 2013.

Address correspondence to:
Dr. Patty J. Lee
Section of Pulmonary, Critical Care and Sleep Medicine
Yale University School of Medicine
P.O. Box 208057
New Haven, CT 06520-8057

E-mail: patty.lee@yale.edu

Date of first submission to ARS Central, September 14, 2015; date of final revised submission, February 21, 2016; date of acceptance, February 22, 2016.

Abbreviations Used

Ad-Ctrl = adenovirus control
Ad-Hsp70 = adenoviral-Hsp70
ALI = acute lung injury

Abbreviations Used (Cont.)

BAL = bronchoalveolar lavage
CD = cluster of differentiation
ChIP = chromatin immunoprecipitation
CT = threshold cycle
DAPI = 4′,6-diamidino-2-phenylindole
DHE = dihydroethidine
DPI = diphenylene iodonium
Duox = dual oxidase
EMSA = electrophoretic mobility shift assay
ERK1/2 = extracellular signal-regulated protein kinases 1 and 2
FACS = fluorescence-activated cell sorter
Hsp70 = heat shock protein 70
IFNα/βRβ = interferon alpha/beta receptor beta
IFNβ = interferon beta
IL = interleukin
IRF3 = interferon regulatory factor 3
JAK1 = Janus kinase 1
JNK = c-Jun N-terminal kinases
LCM = laser capture microdissection
LDH = lactate dehydrogenase
MDA = malondialdehyde
MEK = mitogen-activated protein kinase kinase
miRNA = microRNA
MKK = dual specificity mitogen-activated protein kinase kinase 3
MLEC = mouse lung endothelial cell
mRNA = messenger RNA
Myd88 = myeloid differentiation primary response gene 88
Nox3 = NADPH oxidase 3
p38 = p38 mitogen-activated protein kinases
OCT = optimum cutting temperature
PBS = phosphate-buffered saline
ROS = reactive oxygen species
RT-PCR = reverse transcription–polymerase chain reaction
SD = standard deviation
Ser = serine
sh = short hairpin
siRNA = small interfering RNA
SOD = superoxide dismutase
Stat = signal transducer and activator of transcription
TBARS = thiobarbituric acid-reactive substance
TLR4 = Toll-like receptor 4
TNFα = tumor necrosis factor-α
Trif = TIR domain-containing adapter-inducing interferon-β
TU = transduction unit
TUNEL = terminal deoxynucleotidyl transferase dUTP nick-end labeling
Tyk2 = nonreceptor tyrosine protein kinase TYK2
Tyr = tyrosine
VE-Cad = vascular endothelium cadherin
WT = wild-type